Multi-View Imaging of *Drosophila* Embryos

by

Paul G. Groh

A thesis
presented to the University of Waterloo
in fulfillment of the
thesis requirement for the degree of
Master of Applied Science
in
Civil Engineering

Waterloo, Ontario, Canada, 2008

AUTHOR'S DECLARATION

I hereby declare that I am the sole author of this thesis. This is a true copy of the thesis, including any required final revisions, as accepted by my examiners.

I understand that my thesis may be made electronically available to the public.

Abstract

There are several reasons for imaging a single, developing embryo from multiple view points. The embryo is a complex biomechanical system and morphogenesis movements in one region typically produce motions in adjacent areas. Multi-view imaging can be used to observe morphogenesis and gain a better understanding of normal and abnormal embryo development. The system would allow the embryo to be rotated to a specific vantage point so that a particular morphogenetic process may be observed clearly. Moreover, a multi-view system can be used to gather images to create an accurate three-dimensional reconstruction of the embryo for computer simulations. The scope of this thesis was to construct an apparatus that could capture multi-view images for these applications.

A multi-view system for imaging live *Drosophila melanogaster* embryos, the first of its kind, is presented. Embryos for imaging are collected from genetically modified *Drosophila* stocks that contain a green fluorescing protein (GFP), which highlights only specific cell components. The embryos are mounted on a wire that is rotated under computer control to desired viewpoints in front of the objective of a custom-built confocal microscope. The optical components for the horizontally-aligned microscope were researched, selected and installed specifically for this multi-viewing apparatus.

The multiple images of the stacks from each viewpoint are deconvolved and collaged so as to show all of the cells visible from that view. The process of rotating and capturing images can be repeated for many angles over the course of one hour. Experiments were conducted to verify the repeatability of the rotation mechanism and to determine the number of image slices required to produce a satisfactory image collage from each viewpoint.

Additional testing was conducted to establish that the system could capture a complete 360° view of the embryo, and a time-lapse study was done to verify that a developing embryo could be imaged repeatedly from two separate angles during ventral furrow formation. An analysis of the effects of the imaging system on embryos in terms of photo-bleaching and viability is presented.

Acknowledgements

I would first like to thank my supervisor, Dr. G. Wayne Brodland, and our lab technicians Caleb Horst and Jim Veldhuis, for the opportunity to contribute to the success of their lab. I am grateful for their encouragement and help over the past few years, it has been a pleasure to work alongside these talented and caring individuals.

I would also like to thank Dr. Bruce Reed in the Department of Biology, and his graduate students, Stephanie McMillan and Roopali Chaudhary, for all their help in setting up the *Drosophila* stocks for our research. They have been very patient and supportive and their assistance was invaluable to this project.

Many thanks to my family and friends for their kindness and support. I am forever grateful for my loving parents and sister, who have always encouraged and supported me to pursue my goals.

To all of the members in our lab group: Tony Leung, Graham Cranston, Justina Yang, Simon Tsui, Abby Li, Jennifer Sweny, Xiaoguang Chen, and the 'honorary' member, Katie Higgins, many thanks for making this experience not only rewarding, but enjoyable as well.

Dedication

I dedicate this thesis to my wonderful family, Mary, Hans and Sonia.

Table of Contents

List of Figures

Chapter 1
Introduction

Embryos undergo dramatic tissue reshaping as they progress through the early stages of development. The cells shift, elongate and move throughout the tissue layers in a series of processes called morphogenesis. The study of these early stages of development is focused on observing cell movement and understanding the forces and biological signaling that drive these motions. The benefit of discovering the forces involved with morphogenesis is that it helps researchers understand the process of normal embryo growth. Characterizing morphogenesis will also help understand the cause of malformation-type birth defects, possibly leading to methods that may prevent these defects from occurring.

There are several reasons for imaging a single, developing embryo from multiple view points. The embryo is a complex biomechanical system and morphogenesis movements in one region typically produce motions in adjacent areas. Previous studies of morphogenesis typically collected time-lapse images from only one viewpoint, making it difficult to grasp the extent of movement throughout the entire embryo [Kam et al., 1991; Minden et al., 1989]. It is very difficult to merge information from different viewpoints of different embryos as embryo-to-embryo differences are too large. However, multi-view imaging of one embryo would document clearly the interconnected cell movements from all areas of a single specimen. An ideal multi-view imaging system would allow researchers to perform surgical procedures, regional drug applications, or genetic manipulations and monitor how other areas in the embryo are affected. High-quality multi-view images can also be processed to create an accurate three-dimensional (3D) reconstruction of the embryo for computer simulations [Brodland and Veldhuis, 1998]. Moreover, a multi-view imaging system allows the embryo to be rotated to a specific vantage point so that a particular morphogenetic process may be observed clearly. The scope of this thesis was to construct an apparatus that could capture multi-view images for these applications.

An excellent test organism for observing embryo morphogenesis is the *Drosophila melanogaster*. Used in many research projects, the genetics of *Drosophil*a are well known and this species has the unique ability to be genetically manipulated for a variety of applications. Transgenic embryos with cadherin and membrane markers are available, allowing for direct imaging of specific areas of the embryo. The modified embryos create proteins that fluoresce and highlight only a few components of the cells, creating more concise images of specific cell movements.

Many embryos (including those from *Drosophila*) are essentially transparent, and to obtain clear images one must image specific planes. A confocal microscope can capture a clear image of a specific focal plane by dramatically reducing the incidence of out of focus light on the image plane. However, confocal microscopes have a specific set of imaging criteria that must be achieved for optimal results. Furthermore, the results from a confocal microscope are prone to optical aberrations and low image intensity. Hence, the best results are produced by using a very sensitive camera and post-processing the images with a software program that uses deconvolution to reverse the effects of blur in the optical path.

In this study, a custom system was built, tested, and used to obtain multi-view images of developing *Drosophila* embryos. The system was able to successfully capture an image set of a complete rotation of the embryo at 20 degree increments. In addition, a 60 minute time-lapse image set of a single embryo from two separate viewpoints was collected. Due to light intensity being lower during collection of confocal images, the fluorescence images collected provided a clearer overview of cell movements.

This thesis contains a literature review about the biology of genetically modified *Drosophila*, confocal microscopy, microscope optics, and image processing methods. This is followed by a section describing the design and layout of the imaging system. Next, the results of the imaging system are presented along with an analysis of the performance of the apparatus and its effect on the development of the embryos. Finally, conclusions and future work ideas are presented.

Chapter 2
Literature Review

In this chapter the basic biology of *Drosophila* is outlined as well as embryo collection and preparation methods. A review of existing three-dimensional embryo imaging is presented. The principles of spinning-disk confocal microscopy and image deconvolution are discussed.

2.1 Biology Background on *Drosophila melanogaster*

2.1.1 Genetic Manipulation

The type of fly that is utilized in our research is the *Drosophila melanogaster*, a common species used for scientific experiments [Roberts, 1986]. The benefit of using *Drosophila* is that they are relatively easy to maintain and daily embryo collection can be accomplished easily using an automated egg collection system. *Drosophila* are unique because they can be genetically modified to express GFP-highlighted cell boundaries at an early age. This enables the visualization of cell shape and cell movements.

In the field of medical research, it is important to observe the interaction of an organism's genetic makeup with the environment. This is known as phenotypic analysis. There are many complex and important factors involved in producing a phenotype including gene expression, and the specific functions of proteins [Hadjantonakis et al., 2003]. Manipulation of genes may be used as a method to cause the malfunction of specific proteins thereby creating developmental defects or other health disorders. Scientists also use genetic manipulation to add markers to proteins such as fluorescent proteins so that cell components may be more easily visualized.

Initially, visual markers were added by microinjecting fluorescently labeled histone proteins directly into the early stage embryos [Kam et al., 1991; Minden et al., 1989]. The proteins would eventually be integrated into the chromatin of the *Drosophila* DNA and carried throughout the embryo well into its later stages of development [Minden et al., 1989]. However, this process involves modifying each embryo before imaging. An easier method is to have the stocks of *Drosophila* genetically modified so that the embryos already carry the fluorescence markers once they become fertilized. Two such modified stocks are now commonly used in embryo imaging; the GAL4-UAS stock and the ubi-DE-cadherin stock.

2.1.2 GFP Expression using GAL4-UAS system

The Green Fluorescent Protein (GFP) is a commonly used protein marker. It is derived from the bioluminescent jellyfish *Aequorea victoria*, and it was first introduced as a genetically stable fluorescent marker in microscopic worms called *Caenorhabditis elegans* (nematode or round worm) [Hadjantonakis et al., 2003]. Many genetic markers can become unstable at elevated temperatures, resulting in loss of luminescence [Hadjantonakis et al., 2003]. Since GFP is stable up to 37°C, it is suitable for use in mammalian systems [Hadjantonakis et al., 2003; Cormack et al., 1986]. Additionally, the GFP does not disrupt the normal growth process allowing for fluorescence imaging in live cells.

The production of GFP in *Drosophila* cells can be accomplished using several gene constructs, one of which is based on the GAL4-UAS system. The first step is maintaining the two stocks of *Drosophila* needed for genetic engineering. In one stock, the *GAL4* gene is added to the *Drosophila* genome [Brand, 1995; Phelps and Brand ,1998]. The presence of the *GAL4* gene allows for GAL4p protein production in the cells. In the other *Drosophila* stock, the *GFP* transgene with GAL4p binding sites is added to the *Drosophila* genome [Brand, 1995]. This special DNA sequence with GAL4 responsive sequences is referred to as the Upstream Activation Sequence (UAS) [Phelps and Brand, 1998]. Since GAL4p is not present in this stock, the UAS-target gene (the *GFP* transgene) is not transcribed [Phelps and Brand, 1998]. The *GAL4* gene and the UAS-target gene are complimentary to each other; the UAS cannot promote *GFP* gene expression without GAL4p [Phelps and Brand, 1998]. Therefore, it is only when these two genetically modified stocks are crossed that the target gene for GFP is expressed in the progeny [Phelps and Brand, 1998]. A promoter or enhancer directs the expression of the GAL4 protein, which in turn activates transcription of the *GFP* gene in the UAS. Figure 1 demonstrates how the two stocks are crossed to create progeny with GFP.

While reliable, this stock does not produce embryos that consistently fluoresce in the early stages of development. It was sufficient for assisting in setting up the optics of the confocal microscope, however there is another GFP expression stock that is more suitable for early stage embryo study.

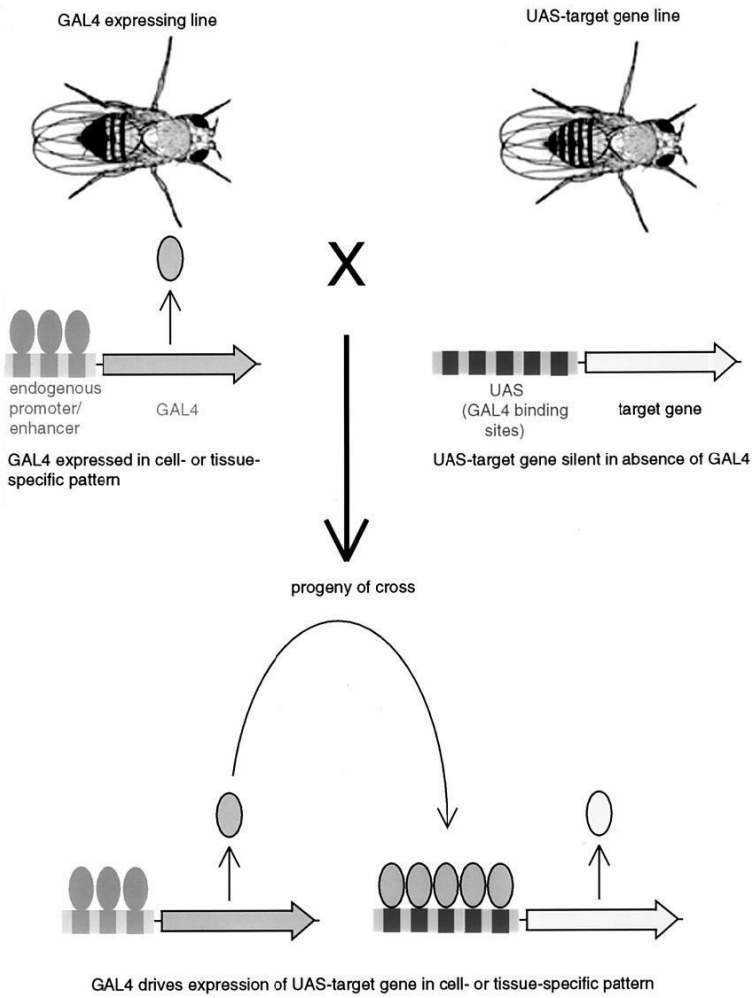

Figure 1: The GAL4-UAS System used to create GFP expressing *Drosophila* [Phelps and Brand, 1998].

2.1.3 GFP Expression using the ubi-DE-cadherin system

The ubi-DE-cadherin-GFP stock contains a specially constructed gene that unlike the GAL4-UAS system, is present in each and every fly. Additionally, the ubi-DE-cadherin-GFP is clearly visible in the cell-cell adheren junctions of blastoderm cells, making it ideal for the study of three-dimensional embryo imaging [Oda and Tsukita, 2000]. Hence, this is the preferred stock of GFP expressing *Drosophila*. The exact process of adding the DE-cadherin-GFP gene to a *ubiquitin* promoter is beyond the scope of this report. However, a more thorough explanation on the construction of the ubi-DE-cadherin-GFP gene is available in the article written by Hiroki Oda and Shoichiro Tsukita [Oda and Tsukita, 2000].

2.1.4 *Drosophila* Life Cycle

This research was targeted at understanding the details of embryo development in the early stages of development (0 – 5 hours after being laid). During this time, the embryo undergoes cell division and cell segregation, the process where the epithelial cells are organized into the outer layer of the embryo. Figure 2 illustrates the changes the embryo undergoes during the first 15 hours of growth.

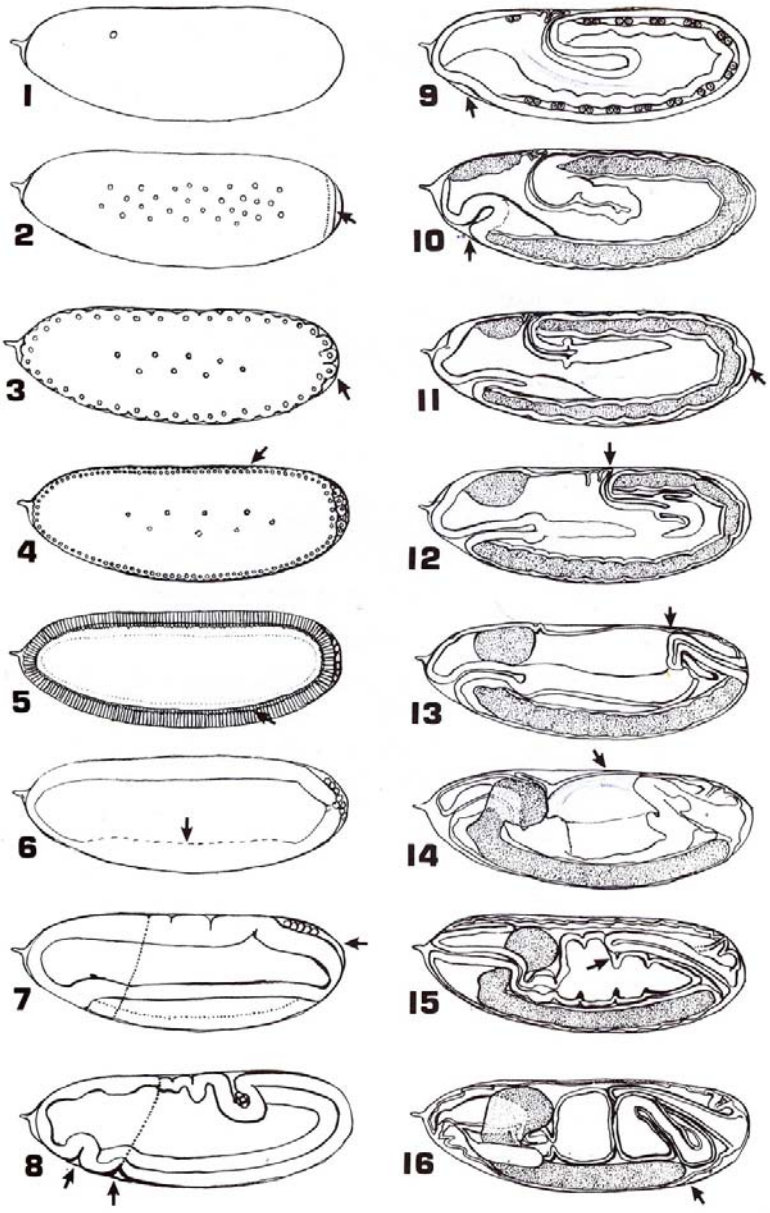

Figure 2: *Drosophila* Embryogenesis from Stage 1 (0 hours) to Stage 16 (~15 hours) [Roberts 1986].

After approximately 22 hours, a larva hatches from the egg. The larva undergoes two moults during its growth before it forms into a pupa around 100 hours after it is hatched from the egg. The *Drosophila* remains as a pupa for another 100 hours while it morphs into the shape of an adult fly. The duration of the entire process from fertilized egg until eclosion (the emergence of an adult fly) is approximately 220 hours at room temperature. The rate of development accelerates at higher temperatures and slows down at cooler temperatures [Roberts, 1986].

2.1.5 Embryo Collection and Sample Preparation

A specific stock of *Drosophila* consisting of 10-20 adult flies in a test tube are transferred into an automated egg collection machine (product name 'FlyMax') by first cooling down the fly stock in a refrigerator for three minutes so that the flies slow down and cannot easily escape as they are moved. The machine is programmed to swap in Petri dishes every three hours for the *Drosophila* to lay their eggs on. The eggs are collected over a three hour time span so that many of the embryos are in the exact development stage for imaging the ventral furrow formation. The Petri dish contains a mixture of agar, grape juice and mould inhibitor to provide an uncontaminated surface where the flies can lay eggs [Reed, 2008]. Additionally, a small amount of moistened brewer's yeast is placed in the center of the Petri dish to promote reproduction.

Each egg has a protective coating called the chorion which must be removed in order to image the embryo with fluorescence microscopy. The chorion reflects many wavelengths of light, making it impossible to distinguish finite details. The fastest way to remove the chorion is to roll the embryo around on a strip of double-sided tape. The glue on the tape pulls the chorion off, separating it from the rest of the embryo. The embryo then has at most 2 minutes where it can be exposed to the atmosphere before it dries out and dies [Brodland, 2008].

Once the chorion is removed, it is possible to determine whether the embryo has been fertilized and can be imaged by the microscope. Moreover, it is possible to determine the stage of development of the embryo. Figure 3 shows the comparison between embryos that have not been fertilized, and embryos that are fertilized and are nearing the desired stage of development.

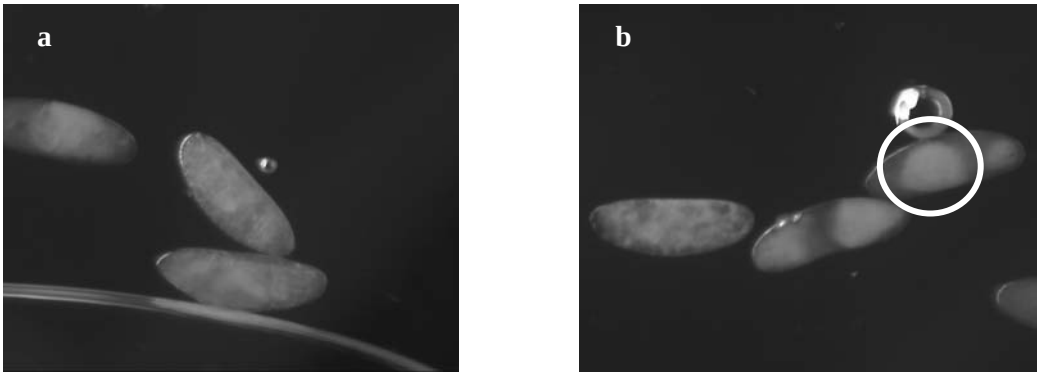

Figure 3: The image on the left (a) shows fertilized embryos developing normally (between Stages 10-13). The image on the right (b) shows three unfertilized embryos that will not develop. Typically, unfertilized embryos will either have large clumps of matter (circled in white), or no discernable interior structure.

It is critical to sort the dechorionated embryos at this point before attaching a wire because it prevents unnecessary imaging of embryos that will not properly fluoresce.

The sorted, dechorionated embryos are quickly mounted to a thin wire using Cyanoacrylate (product name 'Flash - Thick Super Glue'). Once attached, the whole embryo is submersed in a solution of water and salts called '*Drosophila* Ringer' [Roberts, 1986]. This isotonic mixture hydrates the embryo without causing cytolysis and also speeds up the hardening time of the super glue. Once the glue becomes hard and fixed, the embryo is then submersed in a Halocarbon Oil mixture. Halocarbon oil has the unique property of allowing air to pass through to the embryo but it will not let water pass through. Thus, the Halocarbon oil coating protects the embryo and helps it to retain water longer, preventing it from drying out and dying quickly. The oil mixture is a 1:1 combination of two Sigma products, Halocarbon oil 700 and Halocarbon oil 56 [Reed, 2008].

2.2 Three-Dimensional Embryo Imaging

Conventional time-lapse imaging of live *Drosophila* embryos is achieved by mounting a dechorionated embryo on a piece of tape or permeable Teflon membrane, and then covering the specimen in halocarbon oil. A collection of eight to ten optical sections spaced 2 to 3 μm apart is gathered by the imaging system [Hiraoka et al., 1989; Kam et al., 1991; Minden et al., 1989]. The images are then enhanced by sophisticated software to remove unwanted blur and background noise [Kam et al., 1991; Minden et al., 1989]. Some studies have even gone as far as to convert a stack of

optical sections into a three-dimensional array of pixel intensities so that a computer program can generate a pair of stereo images [Minden et al., 1989].

Previous 3D time-lapse imaging studies have focused on observing the dynamics of furrow formation in developing embryos. The 3D time-lapse imaging was accomplished by injecting fluorescent markers into the specimen to highlight cell nuclei, and then capturing a series of optical sections of this modified embryo. The slices were then fed into a computer program that estimated the size and orientation of the cell nuclei and recombined the data into a 3D computer model [Hiraoka et al., 1989; Kam et al., 1991].

There are no existing image collections of *Drosophila* embryos that capture morphogenesis across the entire surface of the embryo. However, a novel approach to 3D reconstruction of live embryos has been accomplished using axolotl (*Ambystoma mexicanum*) embryos [Brodland and Veldhuis, 1998]. The method for imaging these embryos involved using a robotic macroscopic that rotated around the embryo. The viewing angles were chosen so that the 3D position of a feature point on the embryo could be determined using two or more views. Once the critical points were spatially mapped in the computer, an algorithm would reconstruct all of the points into a 3D model essentially capturing the shape and movement of the entire embryo [Brodland and Veldhuis, 1998]. Therefore, the first step in recreating this process for *Drosophila* embryos is to develop a robotic microscope that can capture clear images from multiple angles around the embryo.

2.3 Spinning-Disk Confocal Microscopy

A confocal microscope works by illuminating a small point of the specimen and filtering the returning light through a pinhole or slit before it is collected by a photomultiplier tube [Minsky, 1988]. The small hole only allows light from a specific focal plane to pass through, everything else is blocked from returning to the detector. The specimen is illuminated point by point until a complete image can be formed. By illuminating a small point and not the entire specimen, it is easier to filter out unnecessary light and avoid light from other areas of the sample that might pass through if the entire specimen was illuminated [Minsky, 1988]. Figure 4 illustrates the principle of confocal microscopy.

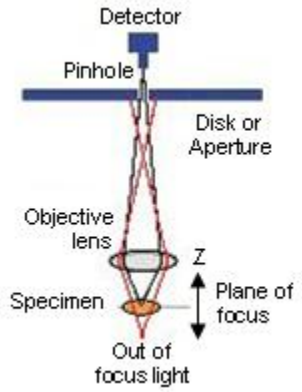

Figure 4: Principle of confocal microscopy, only light from the focus plane is allowed to pass through to the detector ["BD Carv II: Features and Benefits."].

The Scanning-Disk, or as it is also sometimes referred to as the Pinhole (Nipkow) Spinning-Disk Confocal microscope, is an apparatus which allows high-speed collection of confocal images [Xiao, Corle and Kino, 1988]. The disk has many pinholes allowing for several points on the specimen to be imaged simultaneously [Xiao, Corle and Kino, 1988]. Due to the spacing and size of the pinholes, only 5 -7% of the incident light is transmitted through the pinholes to the specimen [Toomre and Pawley, 2006]. Hence, the Scanning-Disk Confocal microscope requires high intensity light and specimens that fluoresce brightly [Toomre and Pawley, 2006]. Figure 5 shows the layout of a Pinhole disk.

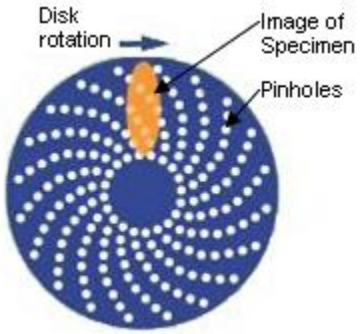

Figure 5: Layout of a Pinhole Disk for confocal microscopy ["BD Carv II: Features and Benefits."]. The orange ellipse is the image of the specimen as projected by the objective.

A molecule fluoresces when it absorbs a photon of light at a shorter wavelength and then emits a photon of light at a longer wavelength [Mallet and Guilabault, 1990]. This event occurs because the

electrons in the molecule are excited by the incident light and transition from their ground state to a higher energy state. When the excited electrons relax to a lower energy state, they emit their energy as a photon. Each excited state has a lifetime associated with it, which determines how long the electron remains in the excited state before it relaxes to a lower energy state [Mallet and Guilabault, 1990]. These fluorescent molecules (also referred to as fluorophores) can be attached to specific parts of a specimen to make them more distinguishable [Hadjantonakis et al., 2003]. The fluorophores can be applied by using either a fluorescent dye to stain a prepared sample or by genetically attaching the fluorescent molecules to the living organism. The emitted fluorescence light will gradually diminish and fade irreversibly, depending on the intensity of the incident light [Diaspro et al., 2006]. Hence, it is important to limit the intensity of the incident light and the duration of the exposure in order to increase the longevity of the fluorophores [Diaspro et al., 2006].

2.3.1 Objectives

Objectives are characterized by their magnification and by their numerical aperture (NA) which is a dimensionless number describing the range of angles that an objective can resolve light into an image [Hecht, 1987]. Equation 1 defines numerical aperture and Figure 6 illustrates the components of the equation:

$$NA = n \sin \theta \qquad \text{Eq. 1}$$

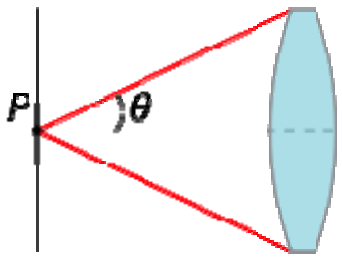

Figure 6: Illustrating numerical aperture. The angle θ, represents the half-angle of the maximum cone of light that can enter the lens.

In Equation 1, the term n is the index of refraction of the medium surrounding the lens, and θ is the half-angle of the maximum cone of light that can enter the lens. As a function of the breadth of angles covered and the index of refraction of the medium being used, NA can also identify the

working distance and the depth of field of the objective [Hecht, 1987]. Generally, as NA increases, the working distance and depth of field decreases.

Objectives also require careful construction in order to minimize chromatic and spherical aberrations. Chromatic aberrations are caused by slight differences in refraction, depending on the wavelength of the incident light [Dunn and Wang, 2000]. Spherical aberrations are caused by slight optical path changes based on the radial distance of the point from the image centre [Dunn and Wang, 2000]. The best possible objectives are planar apochromat, which contain optical elements to correct for longitudinal chromatic aberrations while maintaining a flat image field so that it is possible to gain a sharp view of both the center and the edge of the image across a wide range of colours [Davidson].

2.3.2 Tube Lens

Infinity-corrected objectives project each point in an image as a parallel optical path at a specific angle, as opposed to a conical path converging at a specific point on an intermediate image plane like traditional finite optical systems. In essence, the tube lens collects the parallel light rays emitted by the infinity corrected objective and focuses it at an intermediate image plane. For a spinning disk confocal system, the tube lens is positioned so that the intermediate image plane lies in the pinholes of the spinning disk. Without the tube lens, light from the objective would eventually converge, but the convergence point would be different for every objective. Figure 7 demonstrates the difference between finite and infinite optical systems, and the role of a tube lens for infinity objectives.

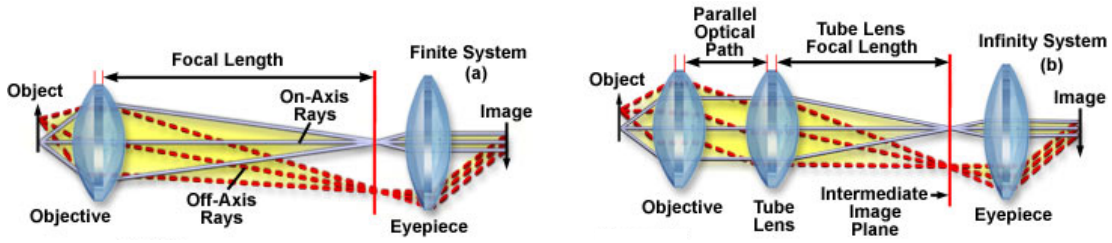

Figure 7: Finite (a) and Infinity (b) Optical Systems [Goulette, Howard and Davidson]. The confocal spinning disk is placed in the position of the Intermediate Image Plane.

The main advantage of this system is that the distance between the objective and the tube lens is not critical. Another advantage is that different image enhancing lenses such as Phase Contrast or Differential Interference Contrast (DIC) can be placed in the Parallel Optical Path without adding any aberrations. Also, a laser beam can be inserted into the Parallel Optical Path, ensuring the beam is

focused on the same point as the image being projected by the objective. This is important for performing cell ablation, which is used in embryonic wound healing experiments [Kiehart et al.].

2.3.3 Resolution and Depth of Field

Light that passes through the pinholes diffracts and undergoes interference in a circular pattern that is commonly referred to as an Airy disk. The process of diffraction and interference limits the resolution of the Confocal microscope to the distance between two Airy disks [Toomre and Pawley, 2006]. The minimum distance required to distinguish between two Airy disks is equal to the radius of one Airy disk, which can be calculated using Eq. 2 where λ_o is the wavelength of the light source and NA_{obj} is the Numerical Aperture of the objective [Toomre and Pawley, 2006]:

$$r_{Airy} = 0.61\frac{\lambda_o}{NA_{obj}} \qquad \text{Eq. 2}$$

The 20x objective in the lab has a Numerical Aperture of 0.75. Using this objective and the GFP light source (520nm wavelength), the smallest resolvable distance is 423nm (0.423 μm). Cell sizes vary in *Drosophila* embryos however many important features are about 10 μm in length, making the resolution of the 20x objective theoretically suitable for our studies.

The theoretical axial resolution of an objective can be calculated using Eq. 3 [Toomre and Pawley, 2006]:

$$d_z = K\frac{\lambda}{n\left[1-\sqrt{1-\left(\frac{NA_{obj}}{n}\right)^2}\right]} \qquad \text{Eq. 3}$$

The variables λ, n and K represent the emission wavelength, the refractive index of the medium and the scalar correction factor, respectively. For small pinholes, the scalar correction factor, K, is set to a value of 0.67. Again, using the 20x, 0.75NA objective in air (refractive index = 1) and the GFP light source, the axial resolution is approximately 1029nm. The GFP light source is Metal Halide lamp with a GFP bandpass filter [product name 'X-Cite']. However, this equation underestimates the actual depth of field because it does not account for out-of-plane light that passes through other pinholes, thereby degrading the image [Toomre and Pawley, 2006]. Published values for laser

scanning confocal microscopes using 0.75NA objectives list their axial resolution at 1.5 μm [Inoue, 2006].

2.3.4 Pinhole Sizing

Ideally, the diameter of the pinhole should be the same size as the diameter of the Airy disk produced by the incident light [Toomre and Pawley, 2006]. Anything smaller will unnecessarily block light and reduce the signal-to-noise ratio at the photodetector [Toomre and Pawley, 2006]. Using a pinhole that is larger than one Airy disk allows for collection of more fluorescence light from the specimen, but conversely it also degrades the resolution of the image and may produce pictures that have poorer quality than wide-field microscope images [Cox and Sheppard, 2004].

The ideal pinhole diameter is equal to the full-width half-maximum (FWHM) of the Airy disk produced by the objective [Toomre and Pawley, 2006]. For biological applications, it is necessary to increase this diameter by a factor of two so that it encompasses the first zero of the Airy figure, allowing more light to pass through the pinhole [Toomre and Pawley, 2006]. Eq. 4 is used to determine the ideal pinhole diameter:

$$D_{opt} = \frac{\lambda M}{NA} \qquad \text{Eq. 4}$$

The term λ is the wavelength of light passing through the objective (in μm), and the terms M and NA refer to the magnification and numerical aperture of the objective respectively.

For our applications, the ideal pinhole diameter should correlate with our typical microscope set-up that uses a 20x 0.75NA objective and 520nm (0.52 μm) wavelength light source. According to the above equation, the ideal pinhole diameter for these conditions is about 14 μm, which is smaller than the 70 μm diameter of the pinholes in CARV II. Therefore, the resolution of the images taken by our set-up is impeded by the size of the pinholes. Figure 8 demonstrates the effects of pinholes that are too large.

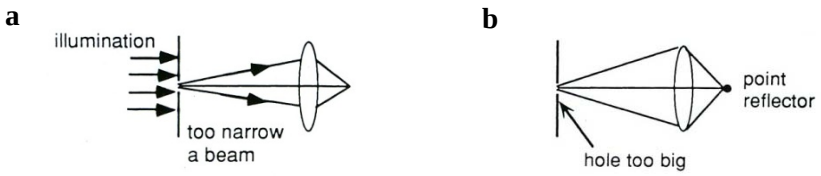

Figure 8: Effect of an oversized pinhole on illumination (a) and emission dection (b) [Toomre and Pawley, 2006].

The large pinhole allows collimated light to pass through but may not diffract light enough to fill the pupil of the objective, causing poor illumination. Furthermore, the larger pinhole will collect more light than required from the focal plane, reducing the z-resolution and giving poor definition [Toomre and Pawley, 2006].

Problems can also occur if the pinhole is too small. Figure 9 demonstrates these errors.

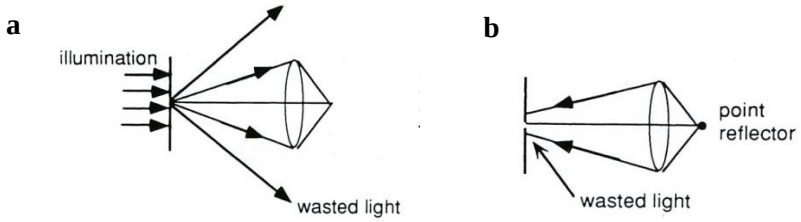

Figure 9: Effect of an undersized pinhole on illumination (a) and emission detection (b) [Toomre and Pawley, 2006].

A small pinhole diffracts the light source too much, causing a waste of light as it overfills the pupil of the objective. Moreover, the pinhole rejects more received light than necessary making the image seem too dark [Toomre and Pawley, 2006].

The pinholes on the Nipkow disk are spaced so that diffracted light from each pinhole does not interfere with the light passing through the surrounding pinholes [Mac Raighne et al., 2005]. However, the spacing between the pinholes on the Nipkow disk is large and the disk reduces the amount of light transmitted to the camera to about 4-7% of the total incident light [Mac Raighne et al., 2005].

2.4 Image Enhancement Methods

Images obtained with a confocal microscope are susceptible to degradation due to non-ideal optics and random noise picked up by the highly sensitive camera system. In order to accurately enhance these images, various corrective models for noise and blur have been developed. Random noise captured by the system is removed by averaging the pixel values in a series of identical images. Meanwhile, a deconvolution algorithm is used to correct for the inherent blur in all of the images.

2.4.1 Averaging Images

The digital camera used to capture the images from the confocal microscope has two primary adjustable parameters: shutter speed and Electron Multiplier (EM) gain. The shutter speed controls the amount of time that the Charged Couple Device (CCD) is exposed to light from the image plane. Generally, this time is kept to a minimum (between 200 to 400 milliseconds) so that a series of photos may be taken before the specimen is altered i.e. moves around, photo bleaches, dehydrates, etc.

The EM gain boosts the incoming signal by sending the incoming electrons through a series of charge-coupled registers, thereby multiplying the number of electrons for the detector to capture [Pawley, 2006]. The net effect of the EM gain is to brighten the image. However it also produces multiplicative noise [Pawley, 2006]. Therefore it is best to keep the EM gain at a moderate level to minimize the amount of multiplicative noise.

Adjusting the shutter speed and EM gain will improve the visualization of small details in the sample, either by increasing the contrast via EM gain or increasing brightness with a longer exposure time. However, manipulating the camera settings can also introduce more additive noise to each frame. A clearer image is produced when eight frames are averaged and presented as one image [Dai and Peng, 1998]. By averaging each pixel value across eight images, most of the additive noise is removed. The improvement made by averaging images is demonstrated in Figure 10.

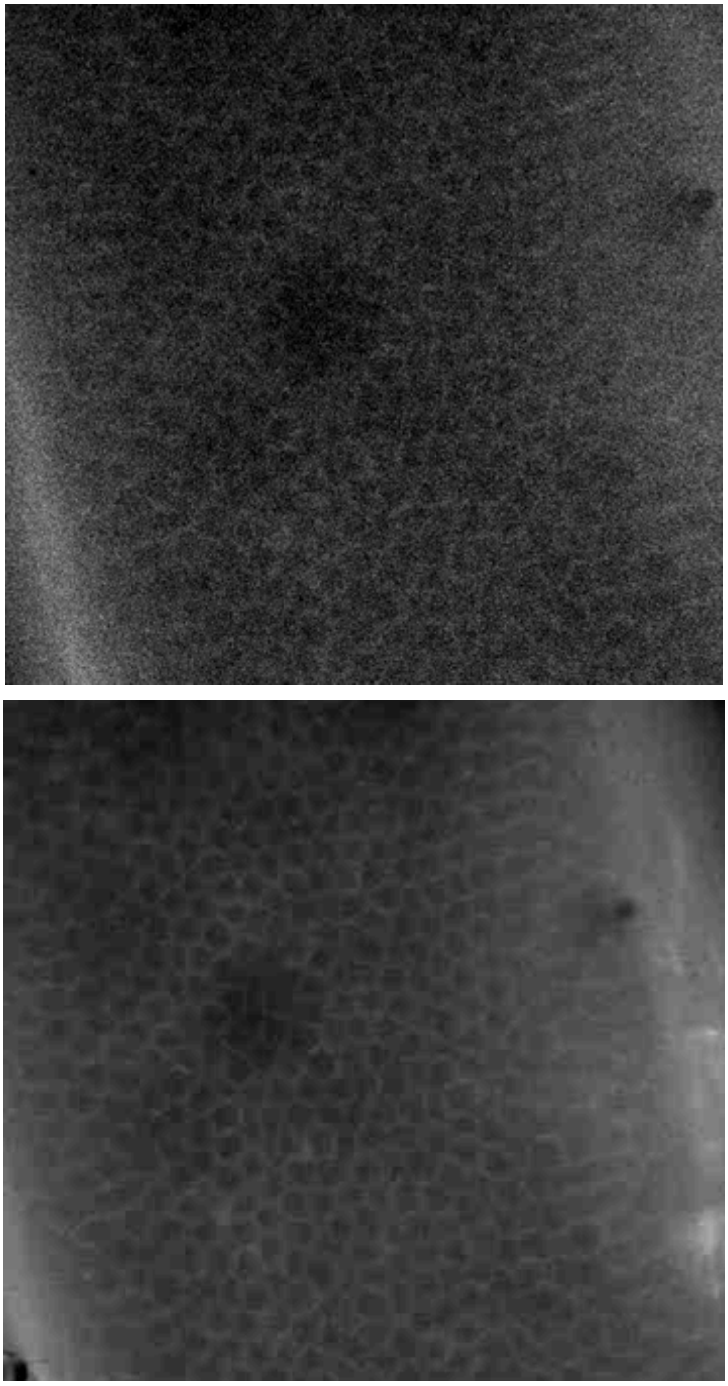

Figure 10: Images of a *Drosophila* embryo in early blastoderm stage. The image on the top is one frame captured by the digital camera while the image on the bottom is an average of eight frames.

2.4.2 Deconvolution of Images

Deconvolution can be used to create sharper images by compensating for blurring due to various effects. Blurring can be caused by many optical components in the light path through a microscope. Primarily, spherical aberration in the lenses is common and can be exaggerated further by changing the refractive indices that the light must travel through i.e. first it must travel through air or glycerol, then the glass cover slip and finally through the mounting media [Shaw 2006]. Also to be considered are the absorption effects in the specimen: the incident beam interacts with different parts of the specimen depending on what point is being imaged and again the light path is slightly altered [Shaw 2006].

Deconvolution attempts to restore an image based on an estimate of the blur introduced in the optical path of the system. An excellent blur model is generated by an ImageJ plugin called 'Diffraction PSF 3D' [Dougherty]. The blur model generates an image called the Point Spread Function or PSF. The PSF represents the picture that would be created by imaging a point source of light. The ideal point spread image would also be a point, but due to imperfections in the system, it is actually a small ellipse with blurred edges. This image can be used with any non-linear deconvolution method.

Two different deconvolution algorithms were used. The first method was the Richardson-Lucy deconvolution method. The Richardson-Lucy method is based on probability and tries to find the maximum likelihood of the image model through an iterative process [Jansson, 1997; Richardson, 1972]. The process is described by Eq. 5.

$$\hat{f}^{(k+1)}(x) = \hat{f}^{(k)}(x) \cdot h(-x) \otimes \frac{g(x)}{h \otimes \hat{f}^{(k)}} \qquad \text{Eq. 5}$$

The variable $g(x)$ is the given image of the original object, h is the blur model and $\hat{f}^{(k)}(x)$ is an estimate of the original object.

The Richardson-Lucy filter is implemented in a computer program using a piecewise approach in the frequency domain [Jansson, 1997]. For a specified number of iterations, r, the filter is applied with Eq. 6 [Jansson, 1997]:

$$\hat{F}_{i,r+1} = \hat{F}_{i,r} \sum_{k=i}^{c} \frac{H_{k-i+1} G_k}{\sum_{j=a}^{b} H_{k-j+1} F_{j,r}} \qquad \text{Eq. 6}$$

Matlab has a Richardson-Lucy algorithm pre-programmed and can be implement using the code line 'deconvlucy'.

The second deconvolution method used was a more advanced program designed for the ImageJ computer platform [available for free on the National Institute of Health website http://rsbweb.nih.gov/ij/index.html]. The 'Iterative Deconvolve 3D' program is based on a Deconvolution Approach for the Mapping of Acoustic Sources (DAMAS) method [Dougherty, 2005]. The exact process behind this method is proprietary information, however the program yielded the best images for study.

2.4.3 Combining Z-Stack Pictures

At high magnifications, the depth of field is relatively small compared to the size of the embryo. In order to capture high-quality pictures of the entire embryo, a series of pictures is taken as the camera moves along an axis perpendicular to the image plane. This axis is commonly referred to as the Z-axis and the pictures collected along this axis are identified as a Z-stack.

A fast method to observe all of the images in a Z-stack is to combine all of the slices into one image. There are several methods to combine pictures by finding the average or maximum value of each pixel in the stack and presenting it as a final image. However these methods include blurred areas that are out of focus as well as background fluorescence thereby creating a final image that includes this spurious information. A more accurate montage can be created by patching together only those parts of the slices that are in focus. This can be accomplished by using the 'Stack Focuser' plugin for ImageJ [Umorin, 2006].

The Stack Focuser algorithm works by running a median filter followed by a Sobel filter on each image to ascertain the best possible edges in each slice. The enhanced images are then processed by calculating the focused edges in a specified region of interest (ROI) and then patching together the ROI's with the best edges into a final image. This is accomplished by finding the maximum pixel value in the ROI and mapping how far the influence of that edge extends across the entire Z-stack. The original slice that contains the maximum pixel value then has the ROI cut out and pasted onto a

final collage image that has repeated the same process, region by region, across the entire image [Umorin, 2006].

The Stack Focuser algorithm is a fast method of combining the Z-stack images, but it does have some limitations. For instance, all of the images must have the same level of brightness otherwise the program will piece together incorrect patches and create artificial edges [Umorin, 2006]. However, the majority of images in the Z-stacks that were processed had consistent brightness levels and most of the information presented in the final collage was not visibly degraded.

Chapter 3
Apparatus Set-Up

3.1 Confocal Microscope Layout

The confocal microscope manufactured by BD Carv is a stand-alone instrument which requires minimal adjustment once installed. The unit is comprised of four disks that can be rotated into a number of different positions. There are two disks that filter passing light into two distinct wavelengths (460nm and 500nm). An intermediate disk is comprised of dichroic filters that reflect light below a certain threshold and transmit light above the threshold. The fourth disk is the Nipkow spinning disk which is patterned with small holes that enables creation of confocal images. A high-speed, high-sensitivity digital camera is attached to the back of the unit to capture the images.

Typically, the confocal microscope is incorporated into conventional upright microscopes, but in order to accommodate the experimental set-ups for this research, a custom horizontal configuration was required. The microscope requires Infinity-Corrected objectives and a tube lens to focus the image onto the Nipkow spinning disk. The spacing between the components is determined by the focal length and Numerical Aperture of the objectives. CFI (Chrome Free Infinity) Nikon objectives were chosen because of their high NA at different magnification strengths. The manufacturer recommended that a tube lens with a focal length of 200mm should be used in conjunction with the objectives in order to obtain the best images [Goulette, Howard and Davidson].

In Figure 11, the layout of the confocal microscope is presented, showing the location of key components and the colour of the light as it passes through different filter sets for GFP imaging. Note that the beam path highlighted in purple illustrates the mixture of blue excitation light and green emission light before the two components are separated at the dichroic mirror.

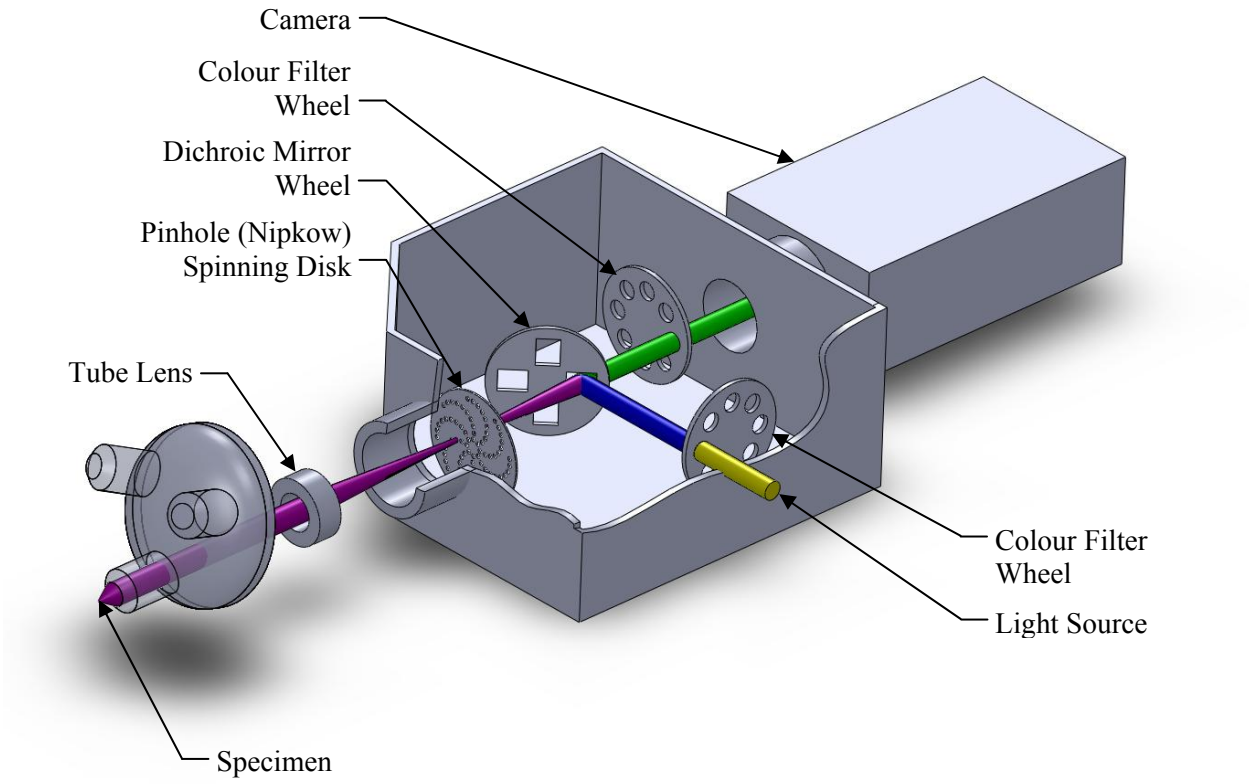

Figure 11: Optical path of the BD Carv II. The beam path highlighted in purple illustrates where the blue excitation and green emission light paths overlap before they are separated by the Dichroic Mirror.

3.2 Embryo Mount

The dechorionated embryos are carefully imaged after they are glued at their anterior or posterior end, to a straight wire and placed in the novel holding tank. Figure 12 demonstrates how the wire and embryo are attached to a rotating motor and placed in a holding tank filled with Halocarbon oil that keeps the embryo alive during observation.

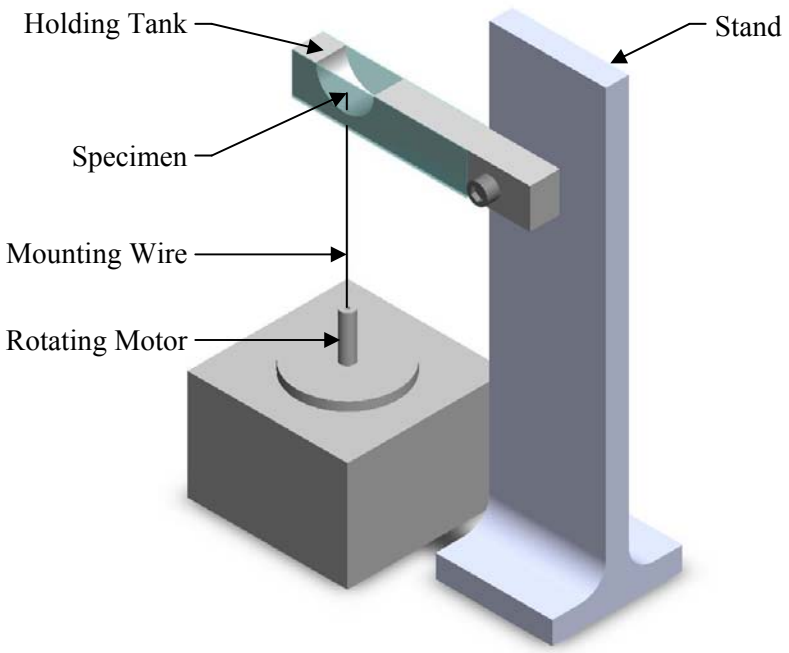

Figure 12: Embryo imaging apparatus.

The holding tank and stand are not attached to the rotating motor so that they may be centered off-axis. In Figure 13, this off-axis orientation is demonstrated from the side view point.

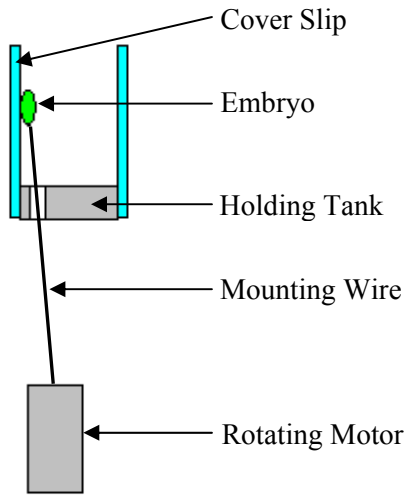

Figure 13: Embryo imaging apparatus, side view showing off-axis orientation of holding tank relative to rotating motor.

The embryo mounting apparatus was designed with this degree of freedom so that the embryo may be more easily pressed against the cover slip at the edge of the holding tank. This is important for imaging since the objective has difficulty focusing on specimens that are not directly behind the cover slip.

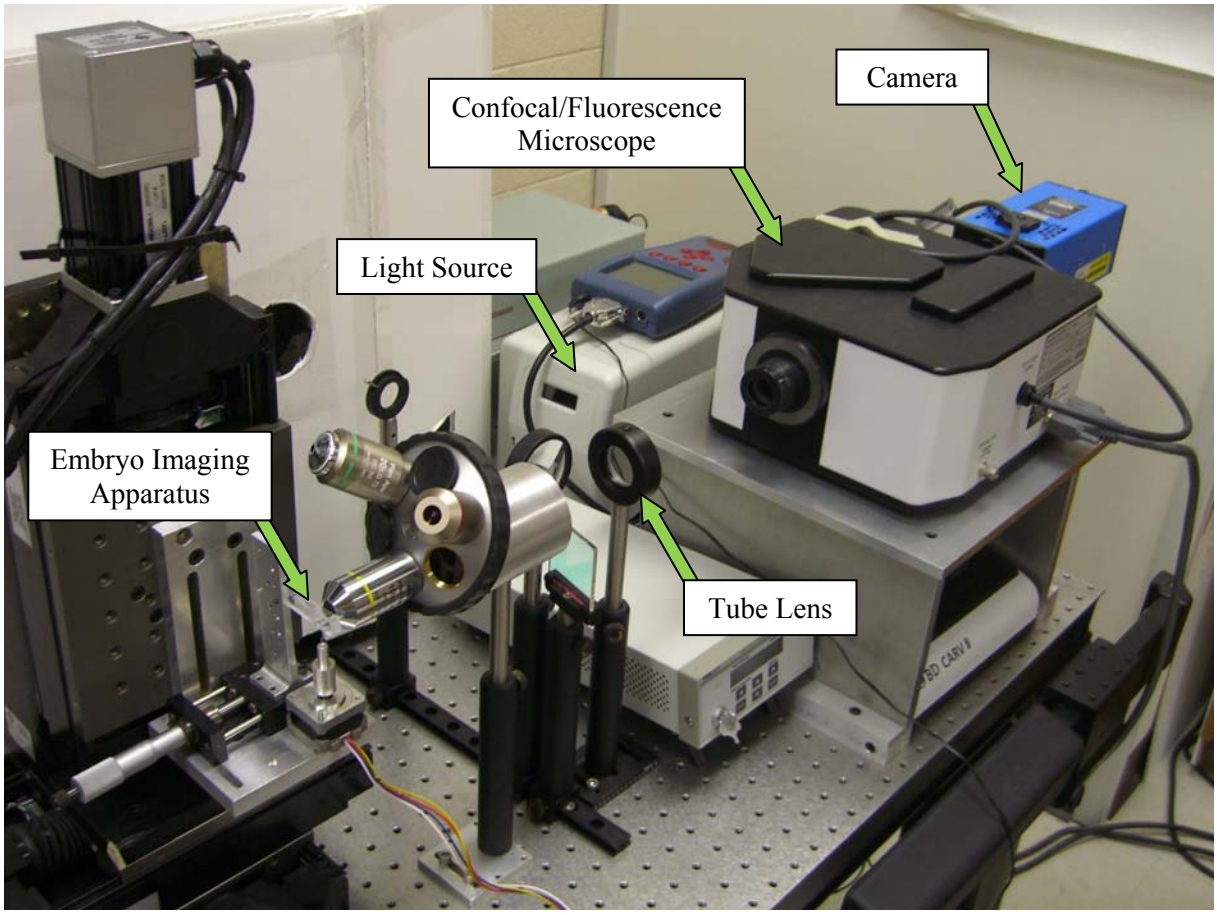

Figure 14: Embryo imaging equipment - dual purpose confocal/fluorescence microscope.

Chapter 4
Experimental Results

4.1 Optimization of image capture

The layout of the new multi-view imaging system is a significant departure from conventional biological microscopy and required several trial and error iterations in order to achieve the desired pictures. The method first involved developing the system to capture images of fixed specimens mounted on a vertical wire and then refining the system to capture image sequences of rotating embryos. This section will review the importance of establishing a suitable optical path and it will compare the images obtained using regular fluorescence imaging with those obtained by confocal microscopy.

4.1.1 Adding a glass coverslip

Originally, the procedure for imaging embryos involved placing the objective directly in front of a specimen that was submerged in protective Halocarbon oil. However, it appeared from the images that the microscope was not capturing images with the same clarity and resolution as it had with prepared, commercially available slides of fluorescing pollen grains [product name 'Carolina Biological Supply Co. Mixed Pollen Grains ']. It was at this point that the embryos were placed behind a cover slip before imaging. The difference in image clarity was significant. Figure 15 compares the results obtained with and without a cover slip. Coverglass compensation optics built into the objective are the most likely cause of this phenomenon.

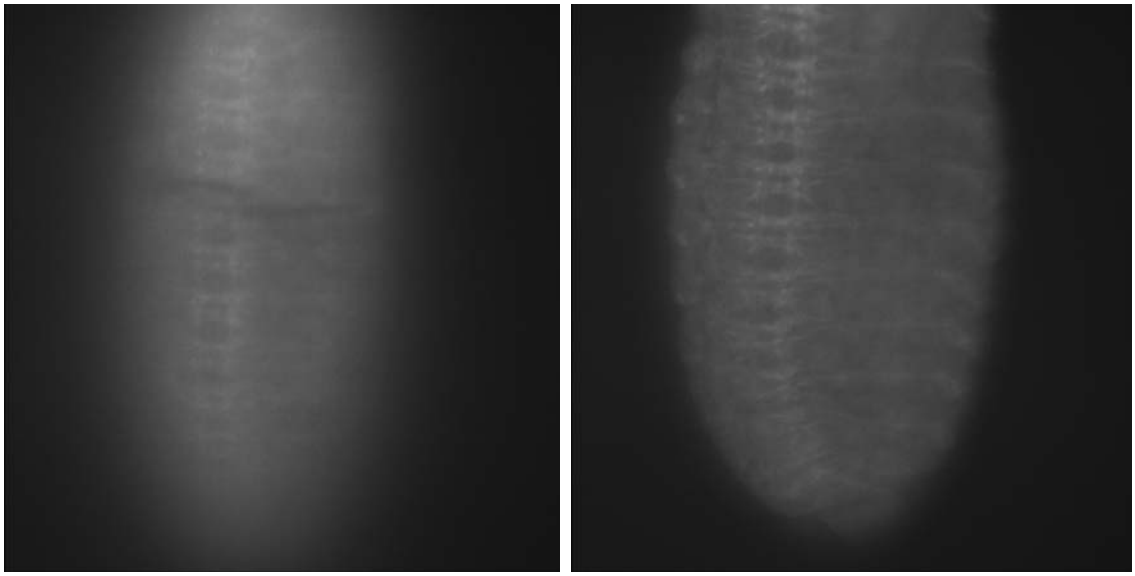

Figure 15: Images obtained without placing a cover slip in front of the specimen (left) have less resolution and clarity then when a glass cover slip is used (right). The embryo being imaged is in Stage 6 (180-195 minutes after fertilization). The image on the right shows more clearly the ventral furrow formation and the transverse folds.

4.1.2 Fluorescence and confocal imaging

Confocal imaging can often improve the resolution of conventional fluorescence imaging by removing out-of-focus light. As described earlier, this process works best with optimally sized pinholes and brightly fluorescing specimens. Ideally, the target would also be thin and pressed closely to the cover slip to reduce the amount of reflection the light experiences before it reaches the objective.

During the initial calibration of the confocal microscope, fluorescing embryos were placed behind a cover slip to ensure that the microscope could gather the best possible image. As Figure 16 demonstrates, the results are very good compared to conventional fluorescence imaging.

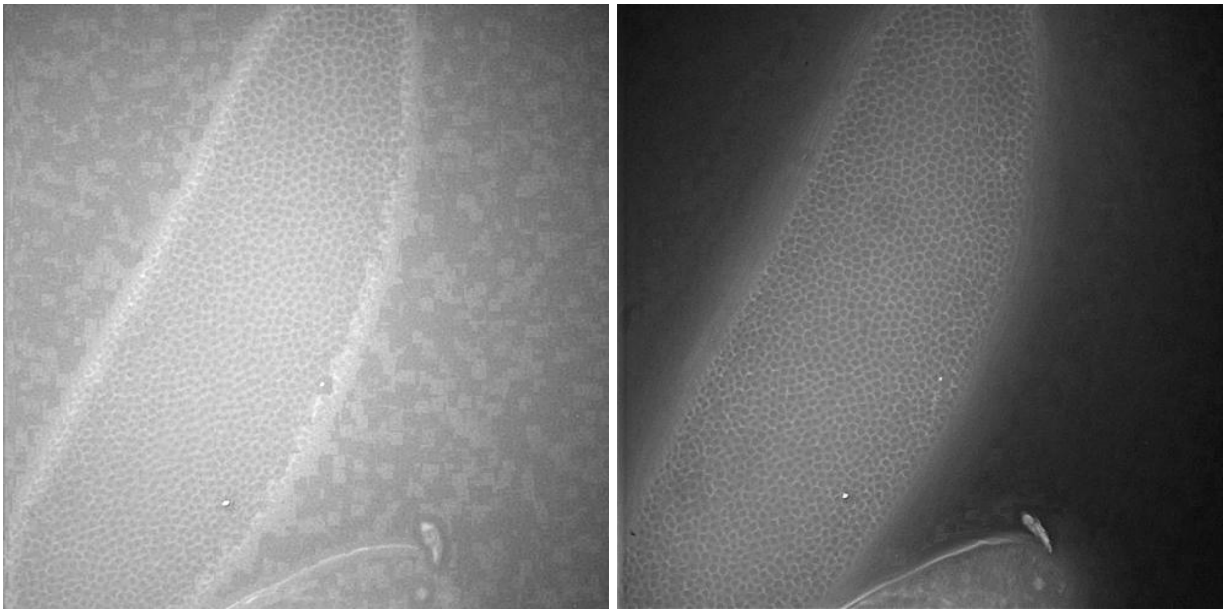

Figure 16: The image collage on the left was created using confocal images, while the image on the right is a collage of fluorescence pictures taken without a confocal disk. The square patches in the background of the confocal image collage are artifacts of the image processing algorithm. There are similar patches in the fluorescence image collage but they are not as noticeable because the background is darker.

Despite the success with the coverslip mounted embryos, the confocal disk did not result in better images of the spinning embryo. Figure 17 contrasts images captured using fluorescence imaging and pictures taken with the confocal spinning disk inserted in the optical path.

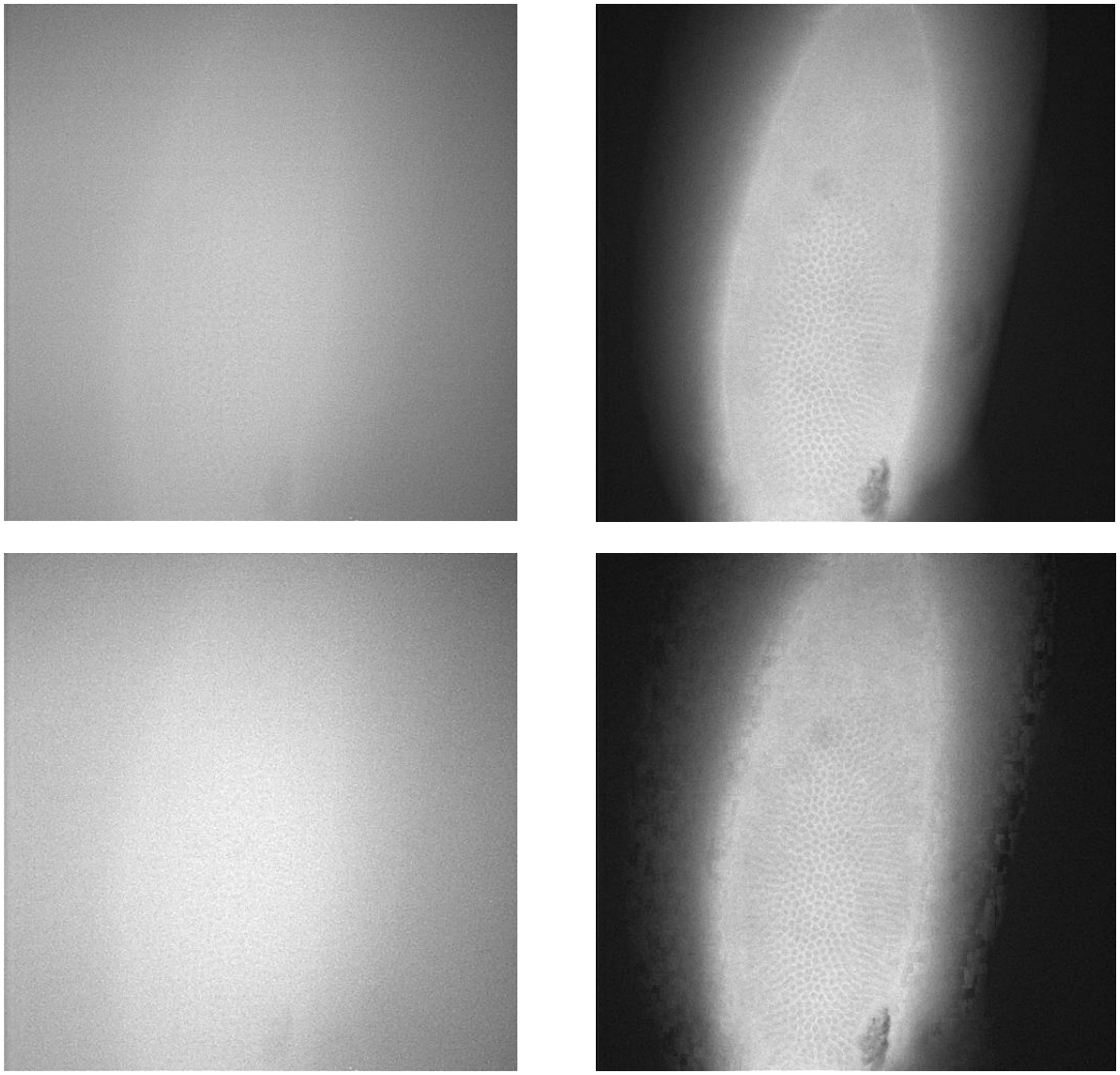

Figure 17: Comparing confocal images (left column) versus conventional fluorescence imaging (right column). The photos in the top row are of an individual optical slice while the photos in the bottom row are an image collage of the Z-stack collected by the two imaging methods. The confocal images in the left column are very difficult to discern, especially when compared to the fluorescence images in the right column.

The confocal results have poor contrast and more noise than the non-confocal images due to a number of factors. First, the EM gain on the digital camera was increased in order to capture the low level of emission light that was returning through the pinholes in the disk. The high EM gain reduced the signal to noise ratio in the images.

Secondly, the genetically modified embryos do not fluorescence as brightly as the prepared slides of dyed specimens that were used to determine the characteristics of the confocal. Thirdly, the embryo is not always pressed up against the cover slip because of the alignment of the embryo with respect to the mounting wire. It is not possible to glue the embryo completely vertical so the embryo is slightly off axis. This means that the fluorescence light must travel through more aqueous medium before reaching the cover slip, increasing the amount of absorption. Figure 18 shows the difference in the alignment of the actual embryo with the ideal placement of the embryo directly behind the cover slip.

Therefore, imaging experiments were conducted without using the confocal disk so that more information about the specimen could be detected. The compromise to using conventional fluorescence imaging is that out-of-focus light interferes with optical sectioning. However, some of the spurious information can be removed with image processing algorithms, providing adequate pictures for feature recognition and tracking.

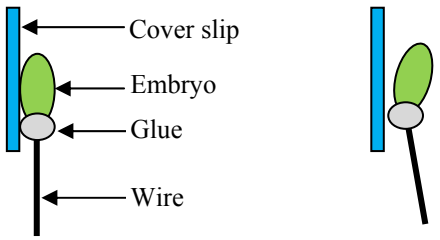

Figure 18: Image on the left shows the ideal placement of the embryo behind the cover slip. The figure on the right is an exaggerated view of how the embryo is actually positioned behind the cover slip.

4.2 Image collage creation

Presenting all the images in a Z-stack can be done effectively by combining all the in-focus sections of the various optical slices into one image. This resulting image is known as a "focus collage" or "extended depth of field" image. The benefit of this process is the generation of a single image where all parts of the embryo are in focus. The major drawback is the number of images that must be taken, which increases the time required to capture a set of images and can result in photobleaching. It was important to choose the number of slices and the spacing between slices carefully to generate quality images in the shortest amount of time.

Originally, the optical slice thickness was set to 1 μm so that highly-detailed data could be collected. However, experiments with conventional 2D embryo imaging can use slice thickness of 1.5 and 2 μm [Kam et al., 1991; Minden et al., 1989]. Therefore, a comparison was done using three different optical slice thicknesses. The results are presented in Figure 19, showing that a satisfactory image collage can be created with an optical slice thickness of 2 or 3 μm. However, the results of the 2 μm slices are desirable because they include less fluorescence data from out-of-focus planes. This is especially evident when viewing the body of the embryo. In the collage created by 3 μm slices, the contrast between the cell membranes and the background is not as good as it is in the collage made by 2 μm slices.

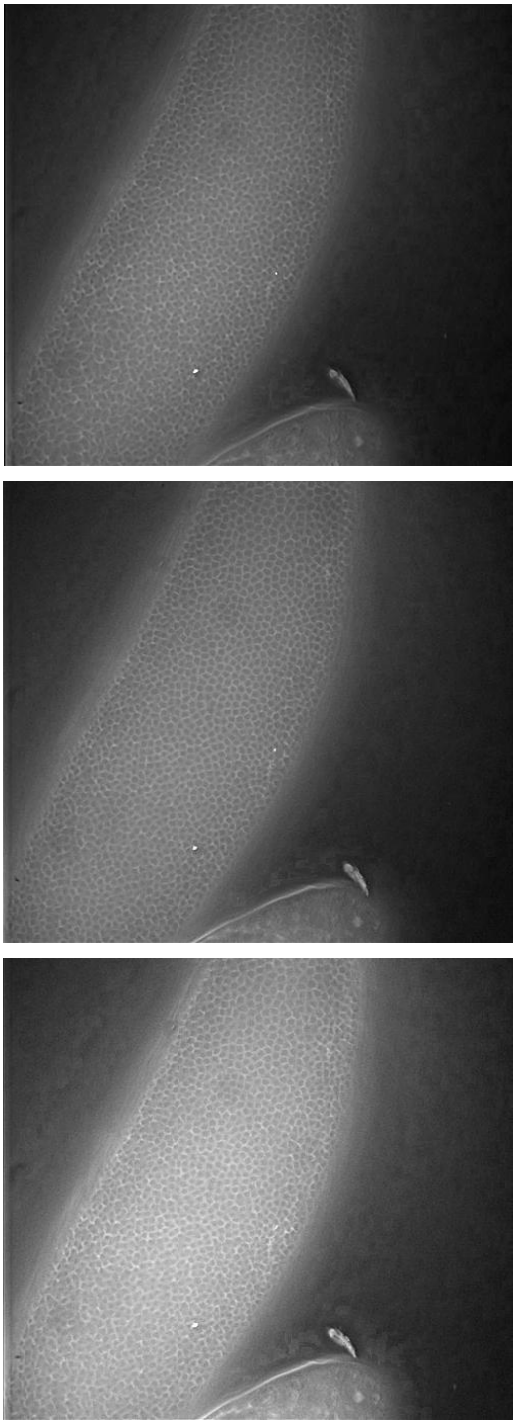

Figure 19: Image collages created using optical slices that are spaced 1 μm (top), 2μm (middle), and 3μm (bottom) apart. The bottom figure has the least amount of contrast between the cell membranes and the background because it is including out-of-plane fluorescence from the other slices.

4.3 Repeatability

For the creation of time lapse data sets where the embryo spins between sets, it is critical that the specimen can be rotated accurately. The ability of the system to return to the same position after each complete rotation was tested using a small piece of glue mounted on the wire where the embryo would normally be placed. The results of this test were positive as the object returned to the same point after every rotation and experienced only minor transverse deviation from its starting point.

Next, two separate types of experiments were designed to find if satisfactory images could be obtained by rotating the embryo through different viewing angles. The first experiment was to rotate the embryo through a complete 360º while the second experiment involved imaging the embryo multiple times at two angles.

4.3.1 Verifying angle rotation repeatability

The ability of the imaging system to accurately rotate the specimen to the same angle consistently was tested using a small piece of glue attached to the mounting wire where an embryo would be placed. The results of this experiment are summarized in Figure 20, noting that the system can return to the same position accurately with only a minor amount of transverse movement.

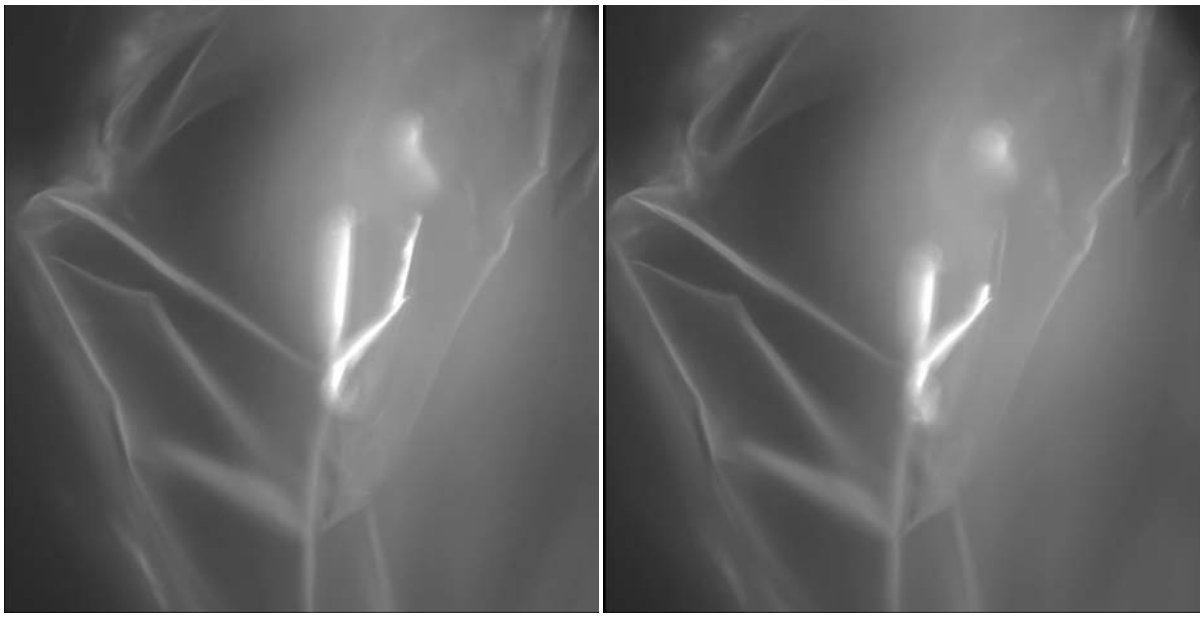

Figure 20: Tracking the change in position of the target as it rotates through 360° repeatedly. The image on the left is the initial placement of the object, while the image on the right is where the object was returned after 80 rotations. The specimen has moved slightly to the left after completing the series of rotations, however, visually, it has returned to the same angle.

4.3.2 Rotating the embryo 360°

The first set of embryo experiments was designed to capture images covering the entire perimeter of the embryo. The success of this experiment was measured by comparing the same group of cells in two separate sets of photos taken from two different angles. In theory, if a group of cells can be imaged from two different angles, then a 3D model of the cells can be created by applying a reconstructive algorithm.

In a study done using axolotl embryos, there were over 700 points visible in at least three views (typically four to eight) thereby creating close to 2800 reconstruction rays that could generate a realistic 3D model [Brodland and Veldhuis, 1998]. The points were observed from images taken at viewing positions on the same horizontal plane as the embyo as well as 45° higher than the original plane and one at 90° to the original plane. The horizontal viewing positions were spaced 22.5° apart, all around the embryo [Brodland and Veldhuis, 1998]. The *Drosophila* embryo was imaged at viewing positions spaced 20° apart to verify that a specific point could be tracked between two or more consecutive angles.

The results of this experiment are presented in Figure 21. It quickly became apparent that tracking individual cells would be very difficult as all the cells share a common circular shape. However, there are large features attached to the outer layers of the embryo that can be used to verify how well the embryo was returned to the same angle after rotating 360°.

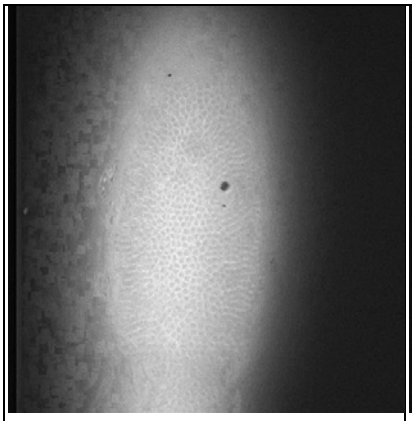	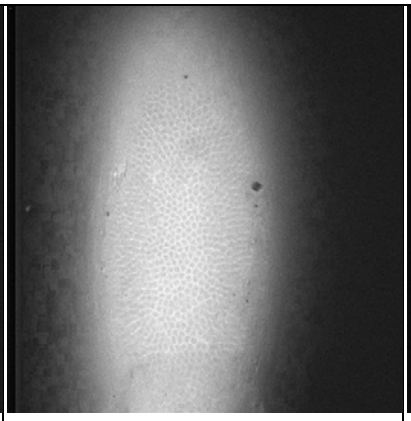	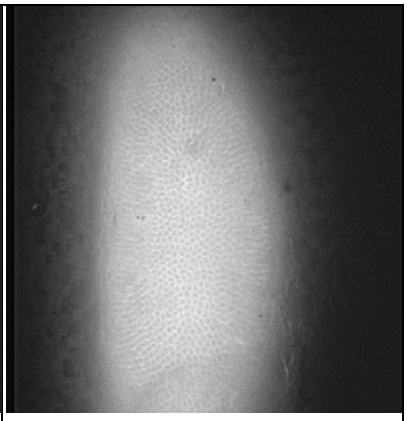
θ = 20º	40º	60º
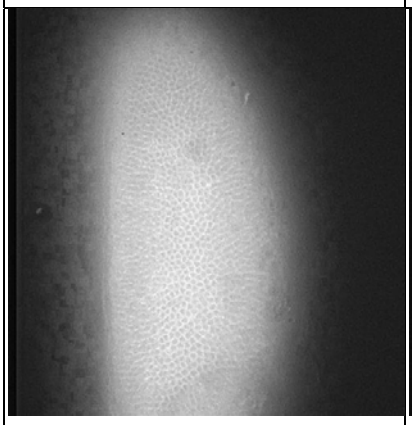	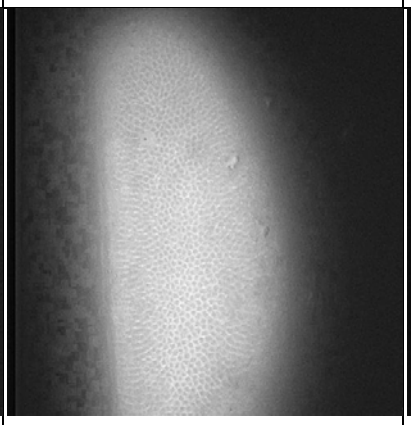	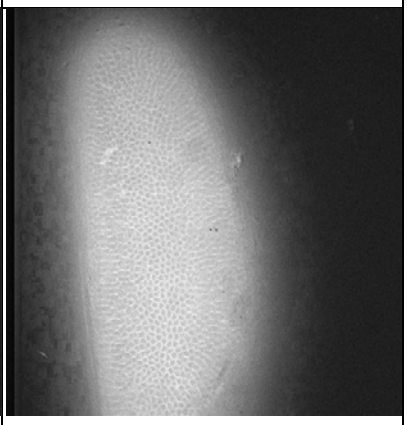
80º	100º	120º
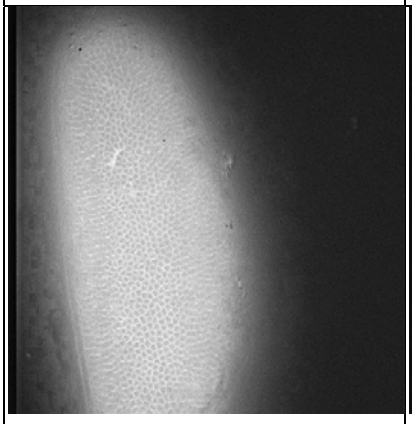	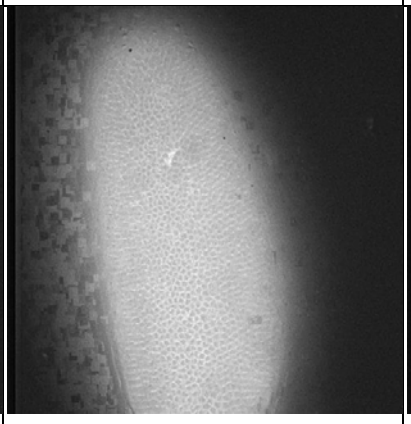	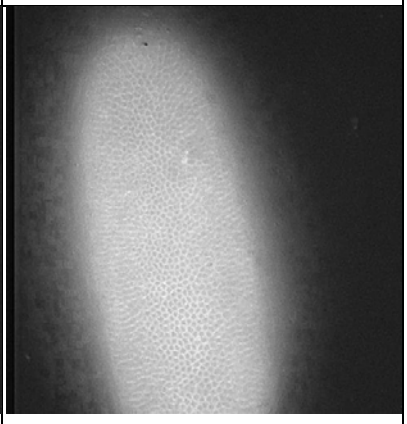
140º	160º	180º

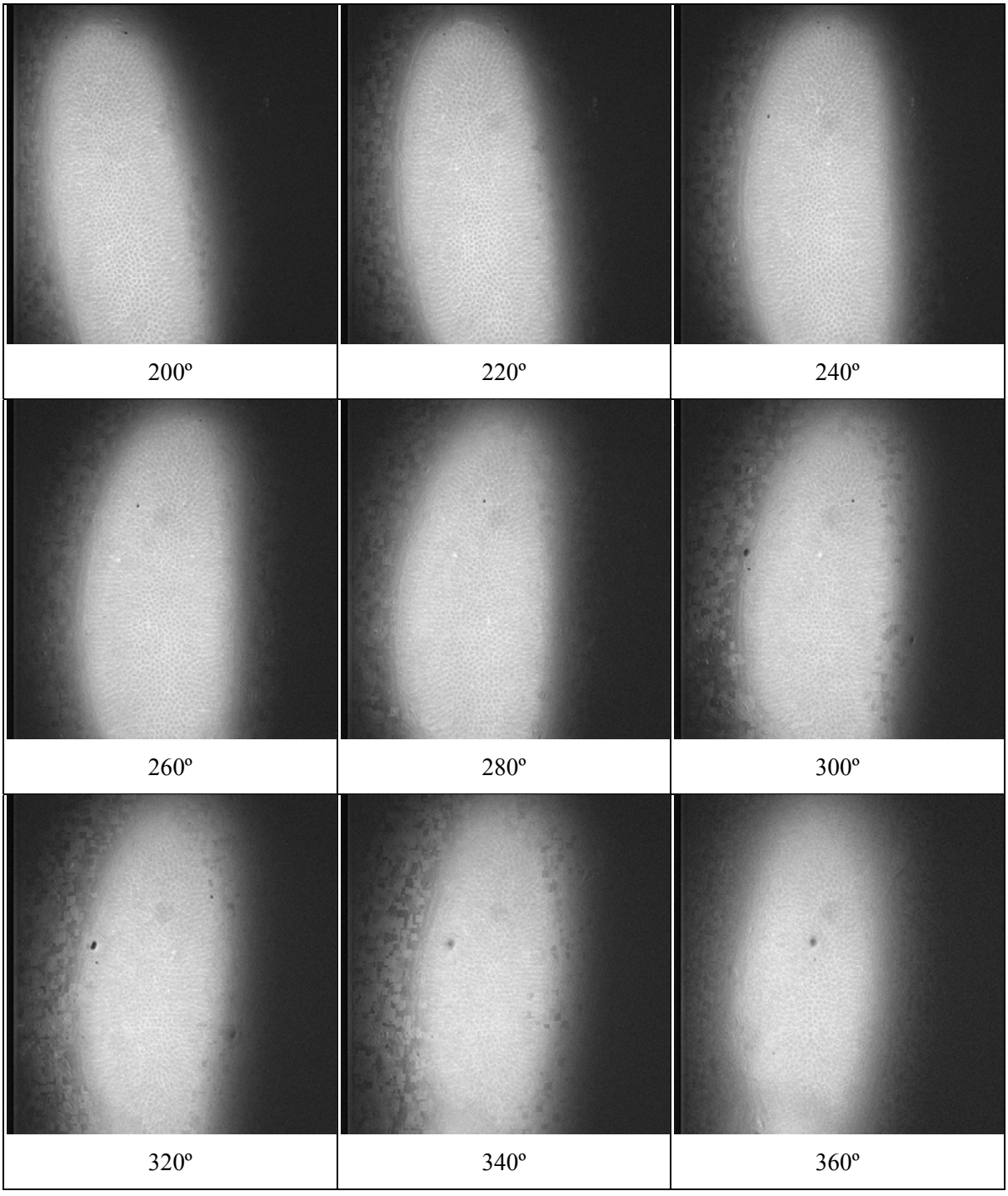

Figure 21: Series of image collages assembled from Z-stacks taken every 20° around 1 embryo. The entire series was captured in about 18 minutes. This embryo was in stage 5 of development (130 to 180 after fertilization).

The experiment could only be conducted for a short amount of time (35 minutes) because the embryo was exposed to the excitation light during the entire process and it suffered from photo bleaching. Another experiment was designed so that the embryo would fluoresce for a longer time frame and provide more feedback into the repeatability of the system.

4.3.3 Time lapse image set at 0° and 30°

This experiment rotated the embryo between two set angles (0° and 30°) and collected a Z-stack at each angle every 2 minutes for 90 minutes. The results are a time lapse collection of an embryo undergoing ventral furrow invagination, a process that when started, moves very rapidly, completing in 15 to 20 minutes [Kam et al., 1991; Leptin and Grunewald, 1990]. The embryo is developing between stages 5 and 6, 130 to 190 minutes after fertilization. A summary of the results obtained by this experiment is presented in Figure 22.

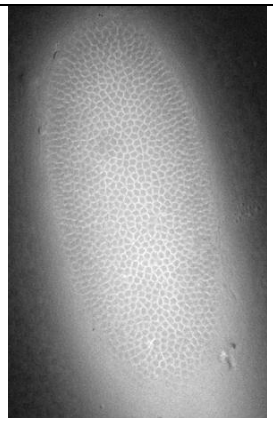 Elapsed time = 8 minutes	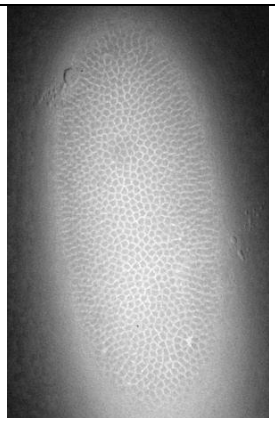	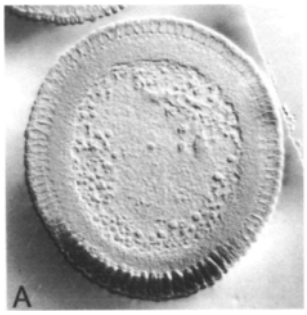
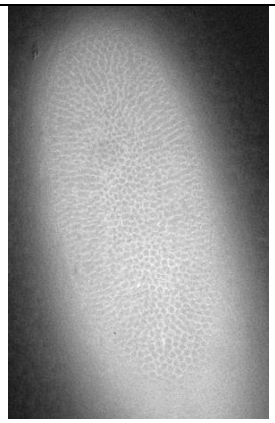 22 minutes	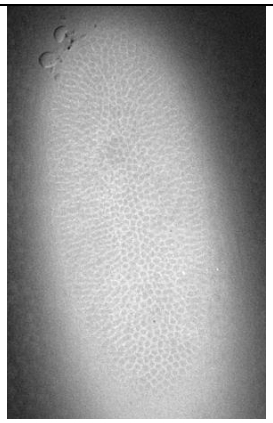	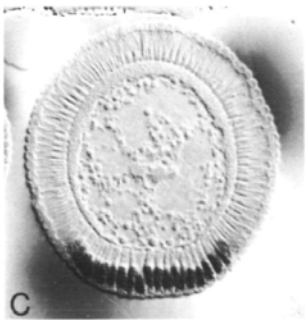
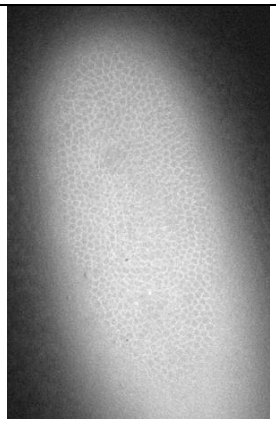 32 minutes	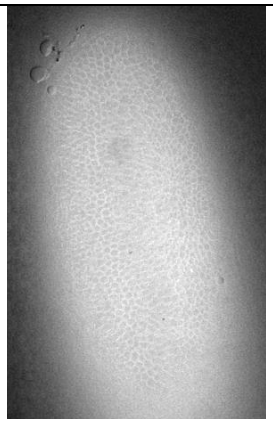	

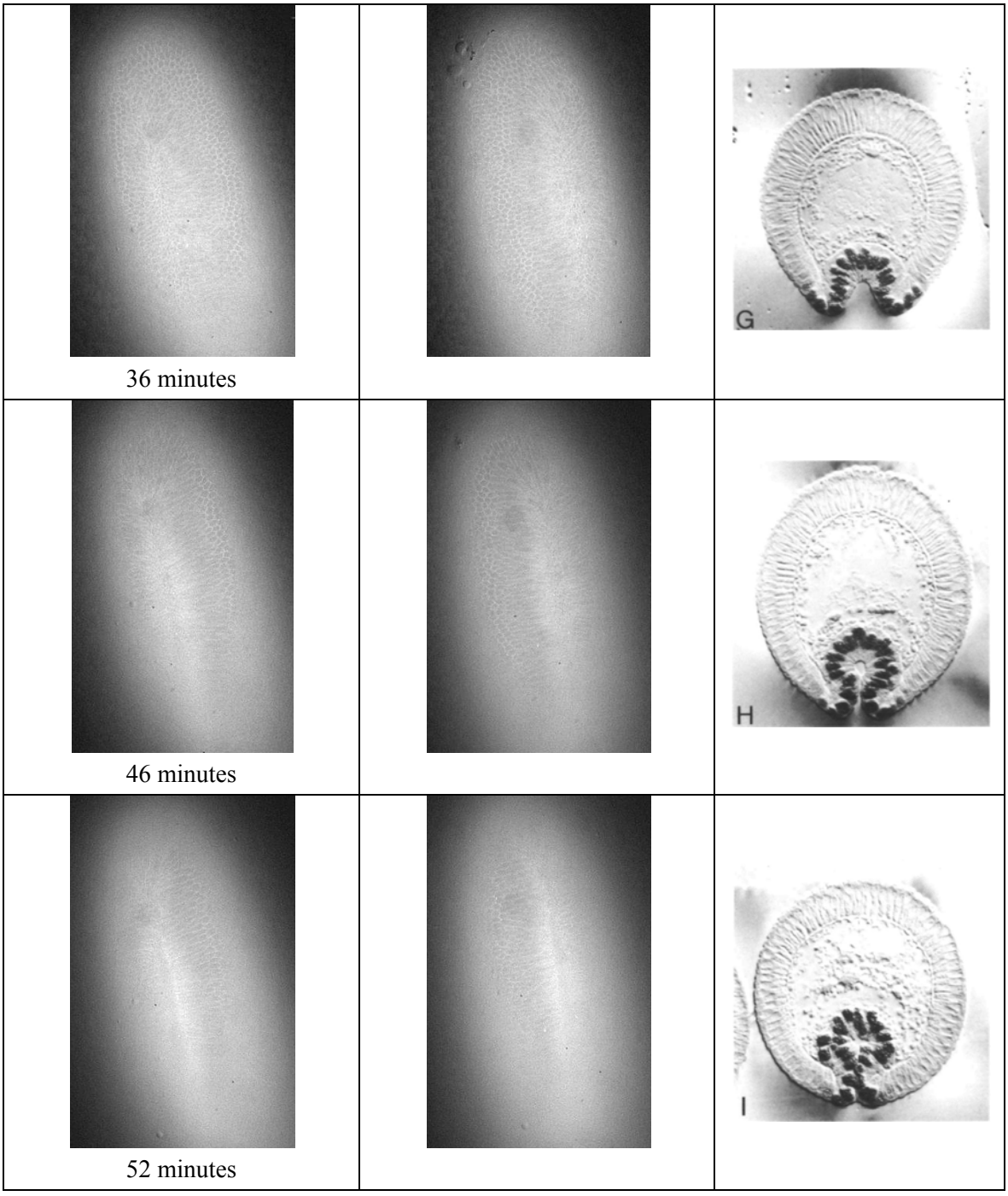

Figure 22: Results of the time lapse experiment compared to cross-sections gathered in the Leptin study (right column) [Leptin and Grunewald, 1990]. The images in the left column are from the 0° reference point and the images in the middle column are from a viewing angle 30° from the 0° reference point. The experimental results are image collages taken at the elapsed time labeled below the picture. Invagination begins at about the 32 minute mark. The results at the end of the experiment (46 and 52 minutes) are not as clear as earlier images because the embryo had moved to a different position in the Z-axis and consequently only one or two successful slices were captured by the automated system.

The changing of epithelial cell shape during invagination has been studied by Leptin and Grunewald in a study that involved physically sectioning embryos during each stage of the furrow formation process [Leptin and Grunewald, 1990]. The images from the Leptin study can be correlated with those obtained during this experiment (Figure 22) to explain what is occurring inside the embryo during the movements captured in the image stacks.

In general, the image collage was able to create a well-focused picture from the Z-stacks taken during the first 20 minutes of the experiment. However, once the cells began the invagination process, the epithelial cells that started with a shallow depth, began to elongate in the z-axis and made it more difficult to create a clear image collage because of the changing cell shapes. The image stacks show the cells tapering to a smaller circumference as the z-slice penetrates deeper into the embryo, which is consistent with the Leptin study (Figure 23).

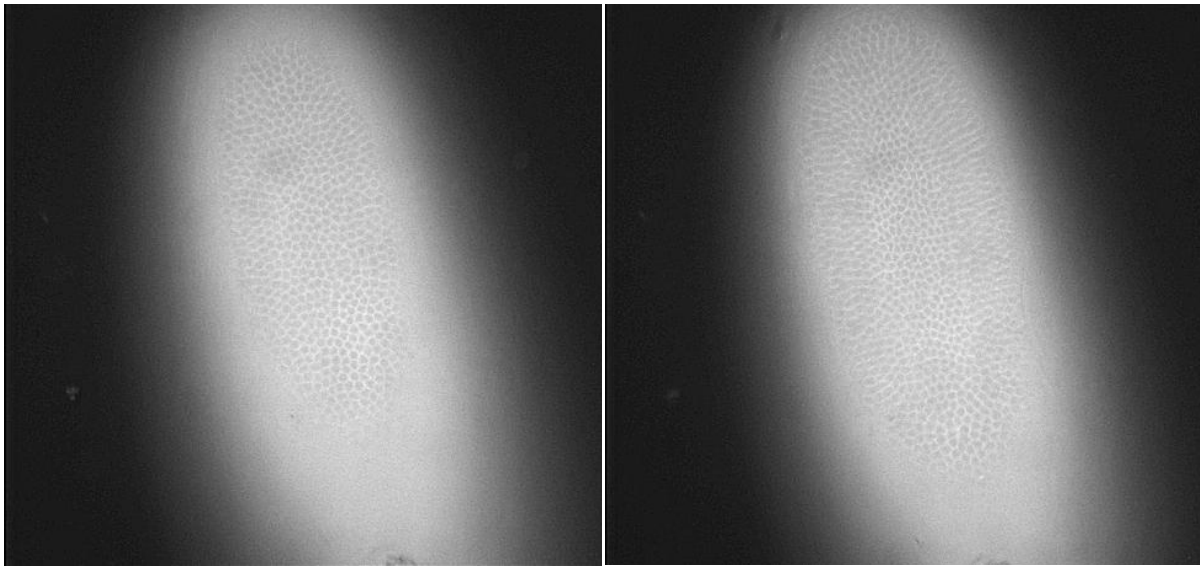

6 μm depth 14 μm

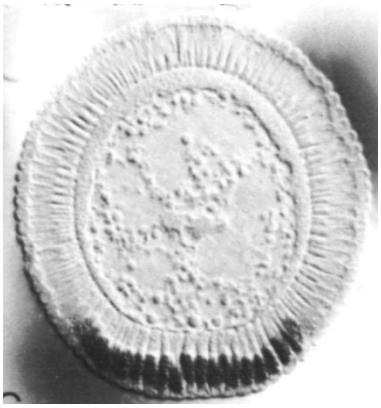

Figure 23: Comparing two image slices (top row) with a cross-sectional view of a developing embryo at approximately the same stage of development (cross-sectional view taken from Leptin article) [Leptin and Grunewald, 1990]. The top two slices were captured from the time-lapse experiment at the 22 minute mark. The average diameter of the cells in the center of the embryo is larger at the 6μm depth compared to the cells in the center of the 14μm slice.

4.4 Photo Bleaching

Depending on the intensity of the microscope light source, the extent of fluorescence in the GFP embryo can be very brief. If the intensity is too strong, the damage to the embryo might even be fatal [Minden et al., 1989]. In order to evaluate the extent of photo bleaching an embryo undergoes, a comparison was made of the average pixel intensity in Z-stacks taken during the experiments. A graph of this comparison is shown in Figure 24.

In the graph, the term 'D.C.' refers to Duty Cycle, which is the percentage of time that the embryo is exposed to the incident light. It can be calculated using Eq. 7.

$$\text{Duty Cycle} = \frac{\text{Amount of time light is on during cycle}}{\text{Total time of cycle}} \qquad \text{Eq. 7}$$

The results of each Z-stack are expressed as the "Average Relative Pixel Intensity" because not every embryo begins the imaging cycle with the same fluorescence intensity. In order to make a similar comparison between imaging cycles, the first image in the Z-stack was chosen as the reference maximum intensity (100% Average Relative Pixel Intensity) and the pixel intensities in all the other Z-stack images were calculated as a percentage of the first picture.

According to Figure 24, the embryo will photo bleach to a similar average pixel intensity, regardless of whether the duty cycle is 100% or 55%. This is not the result that was expected, as it was thought that less light exposure would reduce the photobleaching effect. However, this study was only comparing tests according to the amount of light applied to the specimen and not the location of the light on the embryo. It may be that the embryo cells are opaque and that the test which rotates the embryo completely distributes the incident light evenly around the embryo whereas the other test focuses the light on only two sections and for a longer period of time. For example, one Z-stack of 9 images takes approximately 30 seconds to complete. In the 100% D.C. experiment, one angle of the embryo is exposed to 30 seconds of direct light for the entire 1000 seconds it takes to rotate the embryo. Meanwhile, in the 55% D.C. experiment, the same viewpoint is exposed to direct light 8 times during the same time period for 240 seconds of exposure. The significant increase in exposure time at one viewpoint may cause photo bleaching to occur more rapidly and hence degrade the pixel intensity faster.

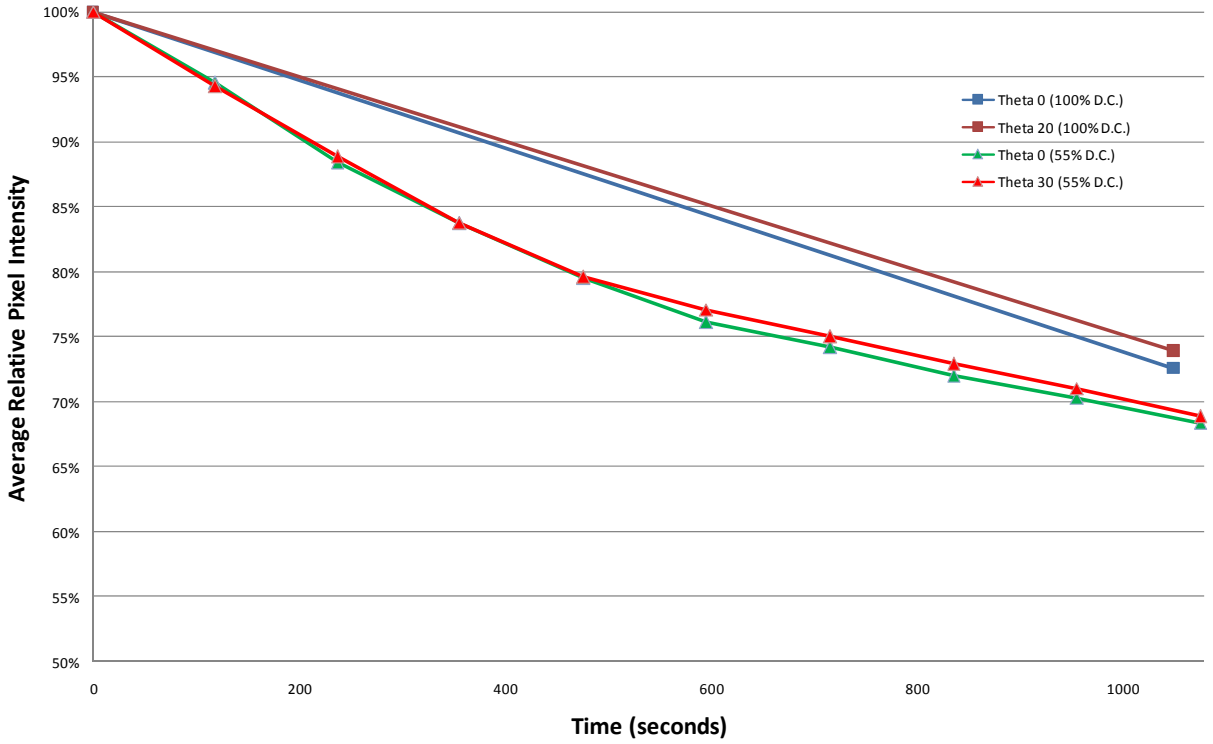

Figure 24: Comparison of decreasing pixel intensities between different Duty Cycles (D.C.). There are fewer points on the 100% D.C. curves because in those experiments, images were captured at 19 theta positions whereas the 55% D.C. experiments only captured images at 2 theta positions. Hence the 55% D.C. experiment was repeated more often in the 1000 second time-lapse compared to the 100% D.C. experiment.

4.5 Embryo viability

An important observation about the imaging methods is noting how long an embryo can develop normally in the apparatus. In the 360° rotation experiment, the embryo did not appear to continue its morphogenesis after 20 minutes, whereas the embryos in the two-angle experiment developed normally during the one hour experiment. However, the embryo did stop development after 1.5 hours and was fluorescing to the same degree as the 360° experiment. Therefore, there is a high level of confidence that an embryo can survive and develop normally in the 360° rotation experiment for about a half hour, and for 1 hour in the two-angle experiment. The short life span may be due to long exposure to intense light.

Chapter 5
Conclusions and Future Work

The multi-view imaging system for live *Drosophila* embryos presented here is the first of its kind. The system was able to image a live, developing embryo from many different angles around its anterior-posterior axis, over time. A key feature of the system is that it consistently returns the embryo to the desired viewing angle even after multiple revolutions.

The system could be refined to image embryos for longer durations, a feature that is important for characterizing morphogenetic movements. Additionally, improvements in the post-processing of images may improve the quality of image collages.

In most experiments conducted using the system, the embryo was kept in the holding chamber for approximately 50 minutes before it became so photo-bleached that it was undetectable through fluorescence imaging, and it stopped development. This time frame was satisfactory for observing rapid developmental events such as ventral furrow formation. However, more testing is required to increase the viability of fluorescing embryos in the apparatus so that longer developmental events may be captured.

When longer time-lapse sets are collected, the embryo may tend to move away from the original focal plane to a greater degree. This problem could be corrected using software that automatically detects when the specimen is moving out of focus and adjusts the focus of the optics accordingly.

Post-processing of the collected image stacks was done using readily available ImageJ algorithms. The deconvolution algorithm was effective in removing much of the blur from the image sets, and the image collage routine could rapidly assemble all of the in-focus sections in the Z-stack and produce one clear image of the embryo. However, the program would sometimes utilize only the last few pictures in the Z-stack. This problem became more apparent during the later stages of ventral furrow formation when the cells elongate in the Z-axis and the Z-stack captures the tapered cell shape in all of its slices. In this case, the larger cell shapes would be ignored by the program and only the last few images would be used in the collage. The program could be improved so that it compensates for thicker cells and utilizes all of the partially-in-focus images in the Z-stack.

In time, data from the system could be used to monitor tissue motions and strains [Veldhuis et al., 2005], characterize cellular fabric [Iles et al., 2007] and make 3D reconstructions [Bootsma and Brodland, 2005].

Appendix A
Preparing Embryos for Observation

First, the chorion must be gently removed from the embryo. This can be accomplished by rolling the embryo across double-sided tape using a pair of tweezers. Once the chorion is removed, the shiny embryo is ready to be affixed to the wire.

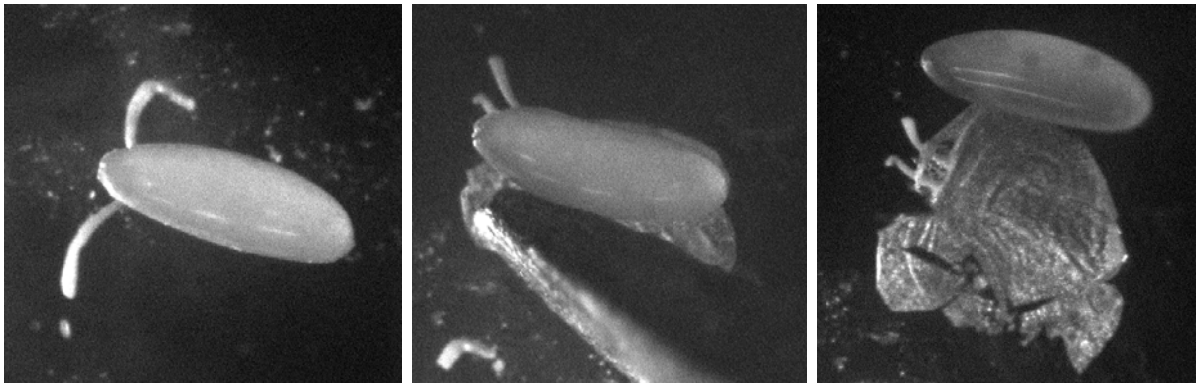

Figure A.1: Rolling the embryo across double-sided tape using tweezers (middle) removes the chorion wrapping from the embryo (right).

The dechorioned embryo is placed on plastic plate that allows part of the embryo to cantilever over the edge so that it may be aligned with the mounting wire. The mounting wire is made of stainless steel and has a diameter of 0.004 inches (approximately 100 μm). The wire is manufactured by Molecu Wire [http://www.molecu.com/].

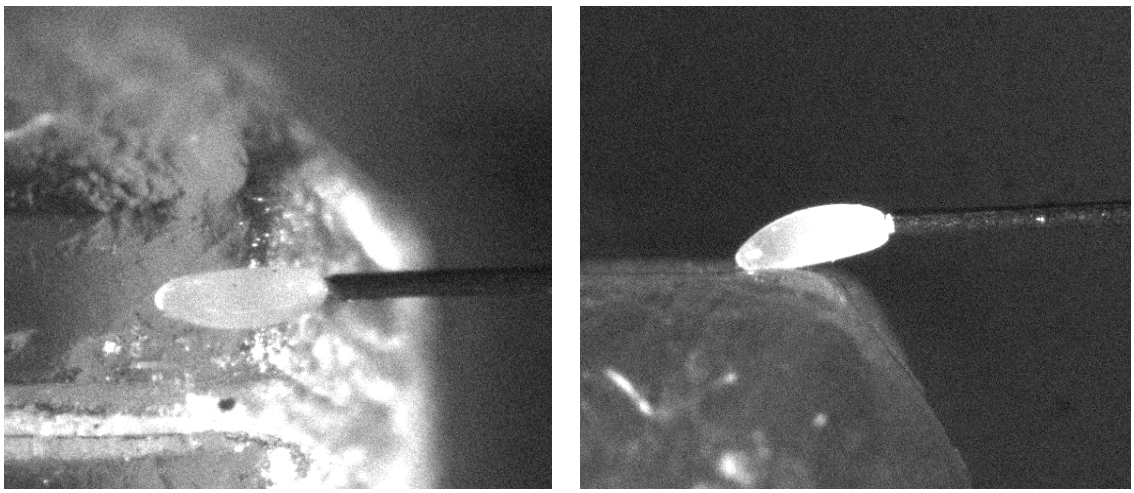

Figure A.2: Aligning the wire with the embryo. The image on the left is a top view and the picture on the right is a side view.

Once the wire is aligned, the glue is applied by dropping a small amount at the junction between the wire and the embryo.

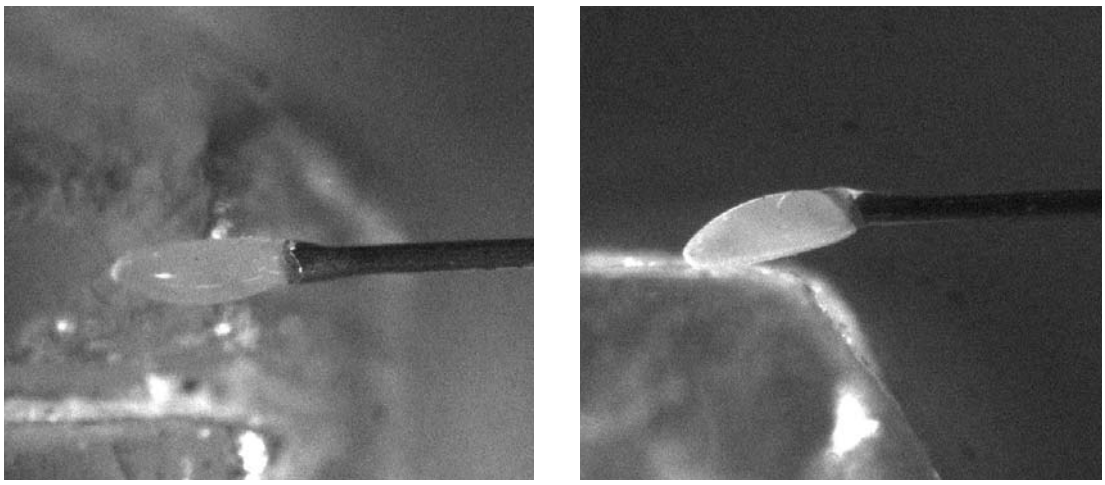

Figure A. 3: Applying glue to the wire-embryo junction. The image on the left is a top view and the image on the right is a side view.

The wire and embryo are rotated 180° so that another drop of glue may be applied to the opposite side. This additional glue prevents the embryo from being pulled askew as the glue dries.

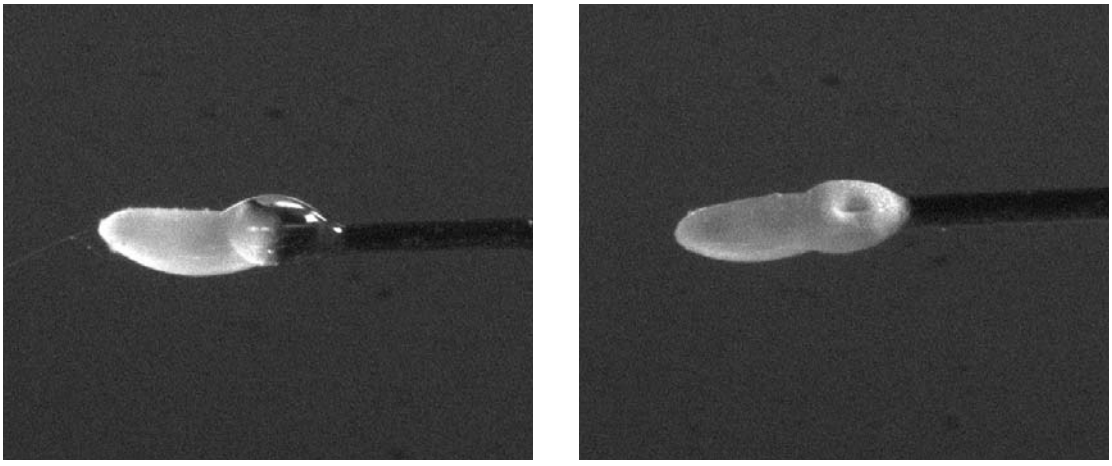

Figure A.4: Glue applied to all sides of the embryo-wire junction. The image on the left has wet glue and the picture on the right shows how the glue dries opaque after being submerged in the isotonic water solution.

References

"BD Carv II: Features and Benefits." Atto Bioscience Inc. <http://www.atto.com/products/carvii/features_benefits.shtml>.

Bootsma, G. J., and G. W. Brodland. "Automated 3-D Reconstruction of the Surface of Live Early-Stage Amphibian Embryos." IEEE Transactions on Biomedical Engineering 52.8 (2005): 1407-14.

Brand, A. "GFP in *Drosophila*." Trends in Genetics 11.8 (1995): 324-5.

Brodland, G. W. Interview: Chorion Removal Methods.

Brodland, G. W., and J. H. Veldhuis. "Three-Dimensional Reconstruction of Live Embryos using Robotic Macroscope Images." IEEE Transactions on Biomedical Engineering 45.9 (1998): 1173-81.

Cormack, B.P., et al. "FACS-optimized mutants of the green fluorescent protein (GFP)." Gene 1.173 (1996): 33-38.

Cox, G., and C. J. R. Sheppard. "Practical Limits of Resolution in Confocal and Non-Linear Microscopy." Microscopy Research and Technique 63 (2004): 18-22.

Dai, Z., and H. B. Peng. "Fluorescence Microscopy of Calcium and Synaptic Vesicle Dynamics during Synapse Formation in Tissue Culture." Histochemical Journal 30 (1998): 189-96.

Davidson, M. W. "Basic Concepts and Formulas in Microscopy: Numerical Aperture." Nikon MicroscopyU. a. <http://www.microscopyu.com/articles/formulas/formulasna.html>.

---. "Microscope Objective Specifications." Nikon MicroscopyU. b. <http://www.microscopyu.com/articles/optics/objectivespecs.html>.

Diaspro, A., et al. "Photobleaching." Handbook of Biological Confocal Microscopy. Ed. J. B. Pawley. 3rd ed. Singapore: Springer Science, 2006. 690-702.

Dougherty, B. "Diffraction PSF 3D - ImageJ Plugin." OptiNav, Inc. <http://www.optinav.com/imagej.html>.

---. "Iterative Deconvolve 3D - ImageJ Plugin." OptiNav, Inc. 2005. <http://www.optinav.com/imagej.html>.

Dunn, K., and E. Wang. "Optical Aberrations and Objective Choice in Multicolor Confocal Microscopy." Nikon MicroscopyU. 2000. <http://www.microscopyu.com/articles/confocal/confocalaberrations.html>.

Goulette, T., C. D. Howard, and M. W. Davidson. "Infinity Optical Systems." Nikon MicroscopyU. <http://www.microscopyu.com/articles/optics/cfintro.html>.

Hadjantonakis, A. K., et al. "Technicolour Transgenics: Imaging Tools for Functional Genomics in the Mouse." Nature Reviews 4 (2003): 613-23.

Hecht, E. Optics 2nd Ed. Reading, MA: Addison-Wesley, 1987.

Hiraoka, Yasushi, et al. "Focal Points for Chromosome Condensation and Decondensation Revealed by Three-Dimensional in Vivo Time-Lapse Microscopy." Nature 342.6247 (1989): 293-6.

Iles, Peter J. W., et al. "Estimation of Cellular Fabric in Embryonic Epithelia." Computer Methods in Biomechanics and Biomedical Engineering 10.1 (2007): 75.

Inoue, S. "Foundations of Confocal Scanned Imaging in Light Microscopy." Handbook of Biological Confocal Microscopy. Ed. J. B. Pawley. 3rd ed. Singapore: Springer Science, 2006. 1-19.

Jansson, P. A. Deconvolution of Images and Spectra. 2nd ed. San Diego: Academic Press, 1997.

Kam, Z., et al. "Drosophila Gastrulation: Analysis of Cell Shape Changes in Living Embryos by Three-Dimensional Fluorescence Microscopy." Development 112.2 (1991): 365-70.

Kiehart, D. P., et al. Ultraviolet Laser Microbeam for Dissection of *Drosophila* Embryos. Duke University:.

Leptin, M., and B. Grunewald. "Cell Shape Changes during Gastrulation in Drosophila." Development 110.1 (1990): 73-84.

Mac Raighne, A., et al. "Variable-Focal-Length Microlens Arrays in Confocal Microscopy." Three-Dimensional and Multidimensional Microscopy: Image Acquisition and Processing XII. San Jose, CA, USA, January 26, 2005.

Mallet, V. N., and G. G. Guilabault. "Fluorescence Analysis of Pesticides and Enzyme-Related Substrates on Solid Surfaces." Practical Fluorescence. Ed. G. G. Guilabault.CRC Press, 1990. 499-542.

Minden, JS, et al. "Direct Cell Lineage Analysis in Drosophila Melanogaster by Time-Lapse, Three-Dimensional Optical Microscopy of Living Embryos." The Journal of Cell Biology 109.2 (1989): 505-16.

Minsky, M. "Memoir on Inventing the Confocal Microscope." Scanning: International Journal of Scanning Electron Microscopy and Related Methods 10 (1988): 128-38.

"Mixed Pollen Grains." Carolina Biological Supply Company. 2008. <http://www.carolina.com/product/mixed+pollen+grains%2C+w.m..do?keyword=pollen+grains&sortby=bestMatches>.

Oda, H., and S. Tsukita. "Real-Time Imaging of Cell-Cell Adherens Junctions Reveals that *Drosophila* Mesoderm Invagination Begins with Two Phases of Apical Constriction of Cells." Journal of Cell Science 114 (2000): 493-501.

Pawley, J. B. "Fundamental Limits in Confocal Microscopy." Handbook of Biological Confocal Microscopy. Ed. J. B. Pawley. 3rd ed. Singapore: Springer Science, 2006. 20-42.

Phelps, C. B., and A. H. Brand. "Ectopic Gene Expression in *Drosophila* using GAL4 System." Methods: A Companion to Methods in Enzymology 14 (1998): 367-79.

Reed, B. Interview: Removing Chorion.

Richardson, W. H. "Bayesian-Based Iterative Method of Image Restoration." Journal of the Optical Society of America 62.1 (1972): 55-9.

Roberts, D. B. *Drosophila*: A Practical Approach. Oxford: IRL Press, 1986.

Shaw, P. J. "Comparison of Widefield/Deconvolution and Confocal Microscopy for Three-Dimensional Imaging." Handbook of Biological Confocal Microscopy. Ed. J. B. Pawley. 3rd ed. Singapore: Springer Science, 2006. 453-467.

Toomre, D., and J. B. Pawley. "Disk-Scanning Confocal Microscopy." Handbook of Biological Confocal Microscopy. Ed. J. B. Pawley. 3rd ed. Singapore: Springer Science, 2006. 221-238.

Umorin, M. "Stack Focuser - ImageJ Plugin." Research Services Branch, National Institute of Mental Health. July 18 2006. <http://rsbweb.nih.gov/ij/plugins/stack-focuser.html>.

Veldhuis, J. H., et al. "Multi-view Robotic Microscope Reveals the in-Plane Kinematics of Amphibian Neurulation." Annals of Biomedical Engineering 33.6 (2005): 821-8.

Xiao, G. Q., T. R. Corle, and G. S. Kino. "Real-Time Confocal Scanning Optical Microscope." Applied Physics Letters 53.8 (1988): 716-8.